Enabling Validation of a CubeSat Compatible Neutral Wind Sensor

Jon Andrew Williams

Thesis submitted to the faculty of the
Virginia Polytechnic Institute and State University
in partial fulfillment of the requirements for the degree of

Master of Science
In
Electrical Engineering

Gregory D. Earle, Chair
Scott M. Bailey
Wayne A. Scales

June 28, 2017
Blacksburg, VA

Keywords: Retarding Potential Analyzer, Microchannel Plate Detector, Atomic Oxygen, Validation

Enabling Validation of a CubeSat Compatible Neutral Wind Sensor

Jon Andrew Williams

ABSTRACT

The Ram Energy Distribution Detector (REDD) is a new CubeSat-compatible space science instrument that measures neutral wind characteristics in the upper atmosphere. Neutral gas interactions with plasma in the ionosphere/thermosphere are responsible for spacecraft drag, radio frequency disturbances such as scintillation, and other geophysical phenomena. REDD is designed to collect in-situ measurements within this region of the atmosphere where in-flight data collection using spacecraft has proven particularly challenging due to both the atmospheric density and the dominating presence of highly reactive atomic oxygen (AO). NASA Marshall Space Flight Center has a unique AO Facility (AOF) capable of simulating the conditions the sensor will encounter on orbit by creating a supersonic neutral beam of AO. Collimating the beam requires an intense magnetic field that creates significant interference for sensitive electronic devices. REDD is undergoing the final stages of validation testing in the AOF. In this presentation, we describe the LabVIEW-automated system design, the measured geometry and magnitude of the field, the specially designed mount, and passive shielding that are utilized to mitigate the effects of the magnetic interference.

Enabling Validation of a CubeSat Compatible Neutral Wind Sensor

Jon Andrew Williams

GENERAL AUDIENCE ABSTRACT

The Ram Energy Distribution Detector (REDD) is a new CubeSat-compatible space science instrument that measures winds in near-Earth space. Gas interactions with plasma in the upper regions of the atmosphere are responsible for spacecraft drag, radio wave disturbances, and other phenomena. REDD is designed to collect direct measurements within this region of the atmosphere where in-flight data collection using conventional spacecraft has proven particularly challenging. The environmental testing needed to demonstrate the sensor requires a specialized system located at NASA Marshall Space Flight Center. To simulate the conditions the sensor will encounter on orbit within a laboratory requires exposing REDD to a supersonic beam of gas using NASA's unique Atomic Oxygen Facility. Forming this gas into a beam requires an intense magnetic field that creates significant interference for sensors such as REDD. Testing in this facility requires a specially-designed sensor mount and magnetic shielding system. REDD is undergoing the final stages of validation testing in the Atomic Oxygen Facility. In this presentation, we describe the computer software-automated system for testing the sensor, the shape and strength of the magnetic field, the specially designed sensor mount, and magnetic shielding that are used to mitigate the effects of the interference.

Dedication

To my parents, Harold and Karen Williams for their guidance, advice, and encouragement to pursue my dreams.

To Ashley McCormick for her firm support and belief in me.

In loving memory of Annie Mae McKeithan and Harold Williams, Sr. without whose influence and belief in advanced education I could not have succeeded.

Acknowledgments

I would like to thank to Dr. Gregory D. Earle for his guidance and patience throughout this mentorship. I would also like to give thanks to the Virginia Space Grant Association for its support through the Graduate STEM Research Fellowship Program. A special thanks is due to Stephen Noel for his mentorship, expertise, and invaluable support throughout work on this project. This thesis was completed due to the endless curiosity and previous work of Lee Kordella in advancing the sensor to the prototype stage. A special thanks is due to Curtis Bahr for his patience, humor, tireless devotion to detail, and long hours operating the Atomic Oxygen Facility. This opportunity would not have possible without the mentorship, knowledge, and support of NASA employees Linda Habash-Krause, Dennis Gallagher, and Jason Vaughn. These acknowledgments would not be complete without the work of my colleague Ellen Robertson for her attention to detail, assistance in testing the device, and persistent optimism.

Funding for this research provided by VSGC and NASA MSFC Cooperative Agreement (Sponsor #:NNM16AA11A)

Unless otherwise noted, all photos by author, 2017.

TABLE OF CONTENTS

LIST OF FIGURES

LIST OF TABLES

LIST OF ABBREVIATIONS

AO = atomic oxygen

AOF = atomic oxygen facility

REDD = Ram Energy Distribution Detector (pronounced "*RED-dee")*

TRL = Technology Readiness Level

LEO = low earth orbit

RWS = Ram Wind Sensor

C/NOFS = Communication/Navigation Outage Forecast System

dt = time step

eV = electron volt

RPA = retarding potential analyzer

MCP = microchannel plate

Bx = *X* component of the magnetic flux density measured by the probe

By = *Y* component of the magnetic flux density measured by the probe

Bz = *Z* component of the magnetic flux density measured by the probe

DI = deionized

GUI = graphical user interface

I/O = input/output

VI = virtual instrument

TDMS = technical data management structure

Introduction

The Ram Energy Distribution Detector (REDD) is a new satellite-borne tool to characterize ion-neutral coupling in the ionosphere/thermosphere. This is achieved through the measurement of neutral gas characteristics including composition, density, temperature, and wind in reference to the orbital track of the spacecraft. Plasma instabilities and neutral winds in this region of low Earth orbit (LEO) are known to affect spacecraft drag, and to cause ionospheric radio frequency scintillation. The critical gap in the science regarding atmospheric interactions in this region has been notoriously difficult to address due to atmospheric density, the practical aspects of spacecraft orbital constraints, and the presence of highly reactive atomic oxygen (AO).

CubeSats have been shown to be a viable choice for exploring this region due to their low-cost and flexibility. The CubeSat-compatible REDD device designed by Virginia Tech is able to collect in-situ measurements within this region of the atmosphere which is prohibitively expensive for large spacecraft. The instrument itself is a derivative of the Ram Wind Sensor (RWS) flown on the Communication/Navigation Outage Forecast System (C/NOFS) satellite (Earle et al., 2007). The size, weight, and power (SWaP) specifications of the RWS have been significantly reduced in the REDD design to enable integration onto standard CubeSat platforms. To enable the device ready for flight by NASA standards, the Technology Readiness Level (TRL) of REDD must be raised from level 5 to level 6. This requires further testing of the instrument prototype in a relevant environment that reproduces the conditions experienced by the sensor in LEO. NASA Marshall Space Flight Center (MSFC) has a laboratory capable of producing a cylindrical supersonic neutral beam of AO in vacuum using their unique atomic

oxygen facility (AOF). Collimating the beam requires an intense 4 kG magnetic field that creates significant magnetic interference for sensitive electronics and the flow of charged particles (Cuthbertson, et al., 1990). REDD is undergoing validation testing in the AOF. In this presentation, we describe the LabVIEW-automated system design, as well as a specially designed mount and passive shielding that are utilized to mitigate the effects of the magnetic interference to enable validation.

Literature Review

The following literature review details concepts that were important to developing a testing system to enable validation of the REDD sensor. It includes review of previous uses of the MSFC AOF system, and a basic diagram of the device. This is followed by a brief review of the RWS and its parentage to the REDD sensor. Lastly, this review will discuss previous progress in prototyping and testing the sensor up to the commencement of this project.

The AOF project at MSFC was begun as a method of producing beams of low energy 3-10 eV neutral atomic for accelerated material testing at Princeton Plasma Physics Laboratory (Cuthbertson et al., 1991). This collaboration between NASA MSFC and the Princeton Physics Department was intended to reproduce the exposure of 5 eV atomic oxygen seen in the LEO environment. This method of performing surface modification studies proved notably successful in simulating the erosion of materials such as Kapton in comparison with Flight experiments aboard STS-8 and STS-41G (Vaughn, et at., 1991). According to plasma emission spectra recorded during the experiments the oxygen molecules experienced nearly complete dissociation into atomic oxygen ions. Composition of the AO beam has been verified through mass spectroscopy and high flux rates of 10^{16} $cm^{-2}s^{-1}$ at targets 9 cm from the neutralizer plate were determined through the use of catalytic probe and material mass loss data. This experimental facility constructed at Princeton under NASA contract was successful enough to warrant the creation of MSFC's own AOF based on this model. The AOF's remarkable capability to simulate extended orbital exposure to 5 eV AO plasma is an essential component in the relevant environmental testing needed to validate the REDD device.

REDD's parentage can be traced to the RWS flown on the C/NOFS satellite from 2008 to 2015. The RWS is intended to study neutral gas characteristics that signal ionospheric plasma irregularities responsible for high frequency radio wave disruption. The device was tested through exposing the device to supersonic fluxes of neutral gas at a specialized facility (Earle, et al., 2007). The RWS's main structural elements include an aperture designed to limit incoming gas particles to a near-normal angle of incidence relative to the spacecraft, charged plates to filter positive ions and electrons, followed by a grid stack. The electroformed meshes that comprise the grid stack function as a retarding potential analyzer (RPA) that's use in ionospheric science has been well documented in Knudsen's 1966 paper regarding this device. The number of ions incident on the channel electron multiplier corresponds proportionally to an output current experienced by the collecting plate (Earle, et al., 2007). This current is measured as a function of the retarding voltage applied to one of the grids within the stack and the resulting I-V curve analyzed using Knudsen's technique. This method of measuring neutral wind characteristics was shown to provide a valuable contribution to exploring variation in ionospheric parameters.

Previous design, fabrication, and testing of the REDD prototype were performed in conjunction with the Creare firm. Without this prior work the current project would not be possible. CAD models of the system were developed iteratively before the various designs were evaluated using the SIMION particle trajectory simulator (Earle, 2015). Iterative simulations of the finalized mechanical design were performed before a prototype device was fabricated and assembled. The prototype underwent extensive in-vacuum subsystem testing followed by static tests of the device using an ion source to verify MCP current scaled as a function of chamber pressure. End-to-end testing of the device was not available without a supersonic neutral gas beam.

Background

REDD Description

The REDD sensor has five key subsystems shown Figure 1: the aperture, extraction plates, ionization chamber, retarding potential analyzer (RPA) grid stack, and the microchannel plate (MCP) . The MCP acts as an electron multiplier (Kordella et al., 2016) to boost the signals to acceptable levels for subsequent analysis. REDD has been designed to admit a supersonic neutral gas beam approaching 7.8 m/s through the aperture, which is ram-facing to ensure that the beam enters at near normal incidence relative to the forward-most plane of the spacecraft. As the neutrals, ions, and electrons enter the aperture at orbital velocity, only the neutrals within the stream are allowed to reach the ionization chamber within the REDD system because the electrically biased extraction plates remove ions and electrons from the incident stream of particles. The extraction plates are located directly behind the aperture, and are biased to ±15 Volts (V) respectively in order to extract the charged particles. Iterative testing in vacuum at fixed pressure showed that these plate voltages are sufficient to prevent the oxygen ions traveling at orbital speed from entering the system. 15 V was found to prevent ~200 eV thermal electrons, and ~5eV positive ions, from biasing the MCP current measurements. The neutral gas components are impervious to the potentials on the extraction plates, and since the mean free path of the particles is large relative to the instrument, the neutrals will continue past the plates and into the ionization chamber.

The geometry of the instrument aperture and the internal ionization chamber aperture ensure that a collimated beam of neutrals is admitted to the ionization chamber. Within this chamber the

neutral particles transect a 100 eV electron beam oriented perpendicular to their direction of travel. Roughly 1 in 10^6 of these neutrals are ionized by the electron beam (Earle, 2015). This ionization efficiency is sufficient to allow detection of the net current in the final stages of the instrument.

These newly created ions then pass through a series of three biased electroformed grids arranged in a vertical stack. These grids comprise the retarding potential analysis (RPA) portion of the instrument. The biased grids serve to attenuate and slow the entering plasma and allow through only ions of sufficient energy levels, as well as collecting any excess electrons from the ionization chamber that could cause measurement irregularities (Fanelli et al., 2015). Plotting the MCP current as a function of retarding voltage applied to one of the grids yields a current-voltage (IV) characteristic that can be analyzed to infer the velocity of the neutral beam relative to the instrument (Knudsen, 1966).

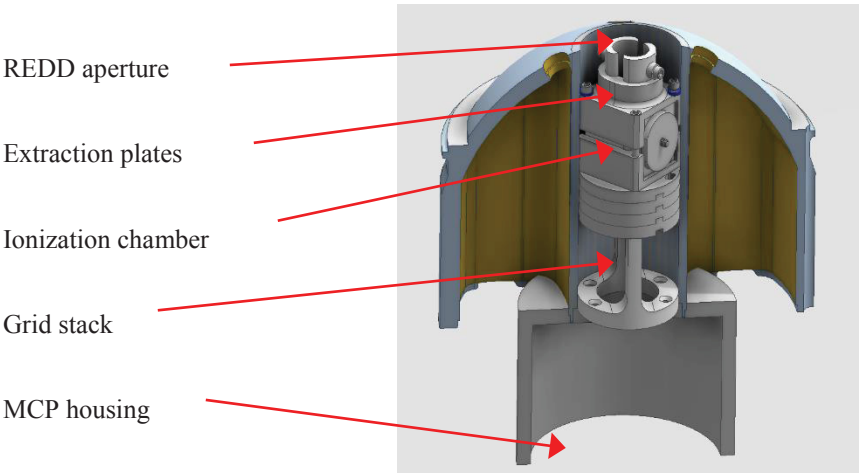

Figure 1: Side View Cutaway of REDD Cad model, with protective dome shield.

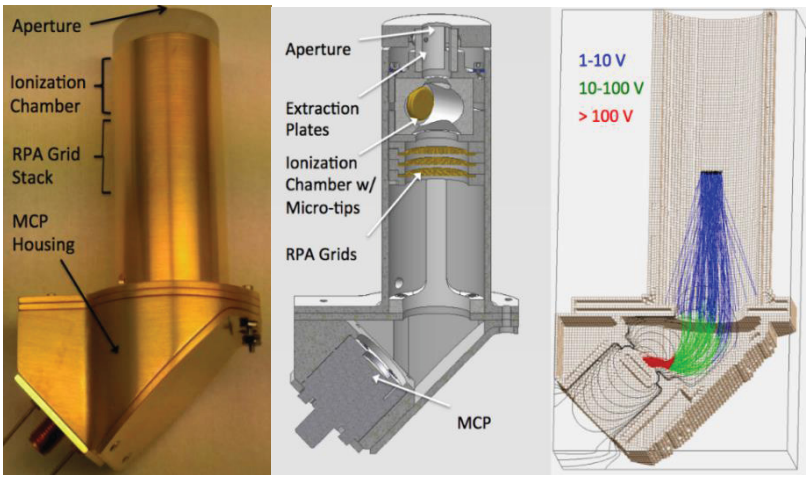

Figure 2 – Side Views of REDD. Left: Gold-plated prototype professionally machined according to Virginia Tech CAD designs. Center: A cut-away CAD design of the REDD showcasing 5 main features. Right: SIMION ™ simulation of electron path from RPA grids to MCP.

Figure 2 depicts a side view of the actual device with scaled versions of both the CAD and simulator results. The right panel of Figure 2 depicts a SIMION ™ simulation of the path of these ions as they accelerate from the final grid to the -2 kV-biased microchannel plate (MCP). The ions enter the 2 mm thick MCP through the many slanted and regularly-spaced tubes comprising the MCP, each of which is only micrometers in size. These micrometer sized channels act as individual electron multipliers due to their surface coatings and the high kinetic energy of the arriving particles. The channels are tilted several degrees relative to the aperture plane in order to ensure the ions strike the channel, causing in a cascade of electrons. This cascade amplifies the signal by roughly 6 orders of magnitude, which is measured by a Keithley 6517b attached to the MCP output as a function of the retarding voltage on the grids. MCP currents in previous LEO applications have been verified to range from ~10-100 nA. REDD's electronics have shown typical noise levels of ~50-100 pA, thereby providing a more than sufficient SNR to produce reliable IV characteristics (Earle, 2015). An example of such an IV characteristic is shown in Figure 3. The neutral state variables (density, temperature, and ram velocity) are inferred from these characteristics through a curve-fitting analysis (Fanelli et al.,

2015). Previous testing of the prototype instrument has shown reliable current measurements in the 100 pA-25 μA range. (Venkatramanan, 2015).

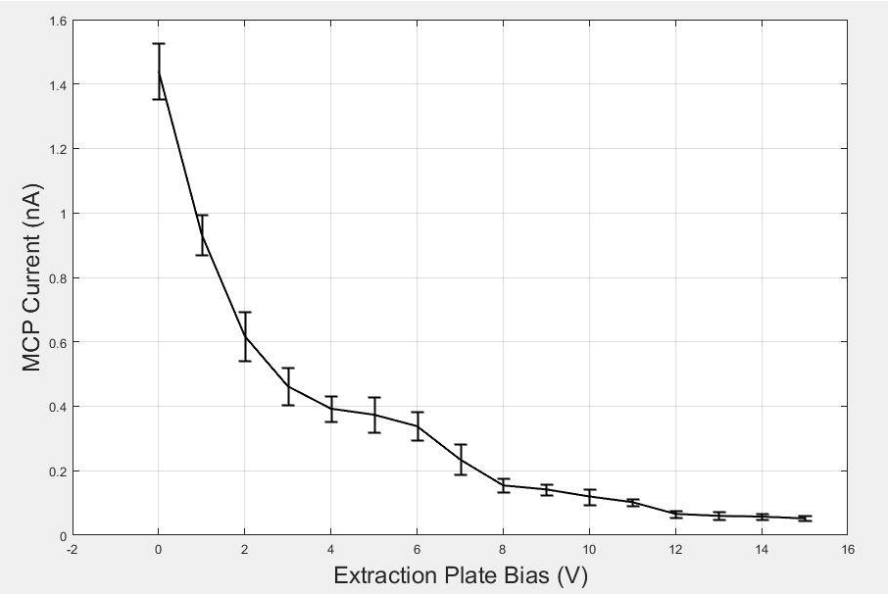

Figure 3: Depicted is an IV curve showing the MCP output current as a function of extraction plate bias (Earle, 2016).

AOF Description

The Atomic Oxygen Facility (AOF) at NASA MSFC is designed for accelerated lifetime materials testing. It is also suitable for REDD validation because it produces a flow of AO at orbital velocities. Relevant environmental testing for REDD involves exposing it to orbital speed monatomic oxygen as expected in LEO at vacuum pressures of approximately $4\text{-}5*10^{6}$ Torr. Figure 4 shows the side view of the system consisting of vacuum chamber, coolant lines, and conducting coils. The REDD system must be mounted to the target cavity, which is the open flange surface shown in Figure 4. The monatomic oxygen is released into the chamber from the rear of the inner chamber located on the right side of the figure, and is reflected from a neutralizer plate angled at 45 degrees towards REDD's intended position at the target aperture.

The pair of conducting coil sets are supplied with 440 A DC at 220 V in order to supply a static 3.4-4 kG magnetic field (roughly 8,000 times Earth's ambient field), to collimate the flow of oxygen ions into a ~1 cm diameter beam. When these ions impact the neutralizer plate they are deflected, and a portion of the population attaches an electron upon impact and becomes neutral. The strong magnetic field prevents the ions from moving away from the central axis of the system, but the neutralized AO beam is not constrained by the field and streams radially outward at high speed toward the REDD aperture.

Deionized water is circulated through the coils during this process to slow thermal buildup within the coils, as any ions in the water would be affected by the magnetic field. A pulsed AO beam is created with Gaussian-distributed density in the radial direction at a ~10 Hz pulse rate. This process imbues the orbital speed monatomic oxygen atoms with the 5 eV level that is analogous to the energy level of oxygen atoms in the atmosphere collected by a LEO satellite.

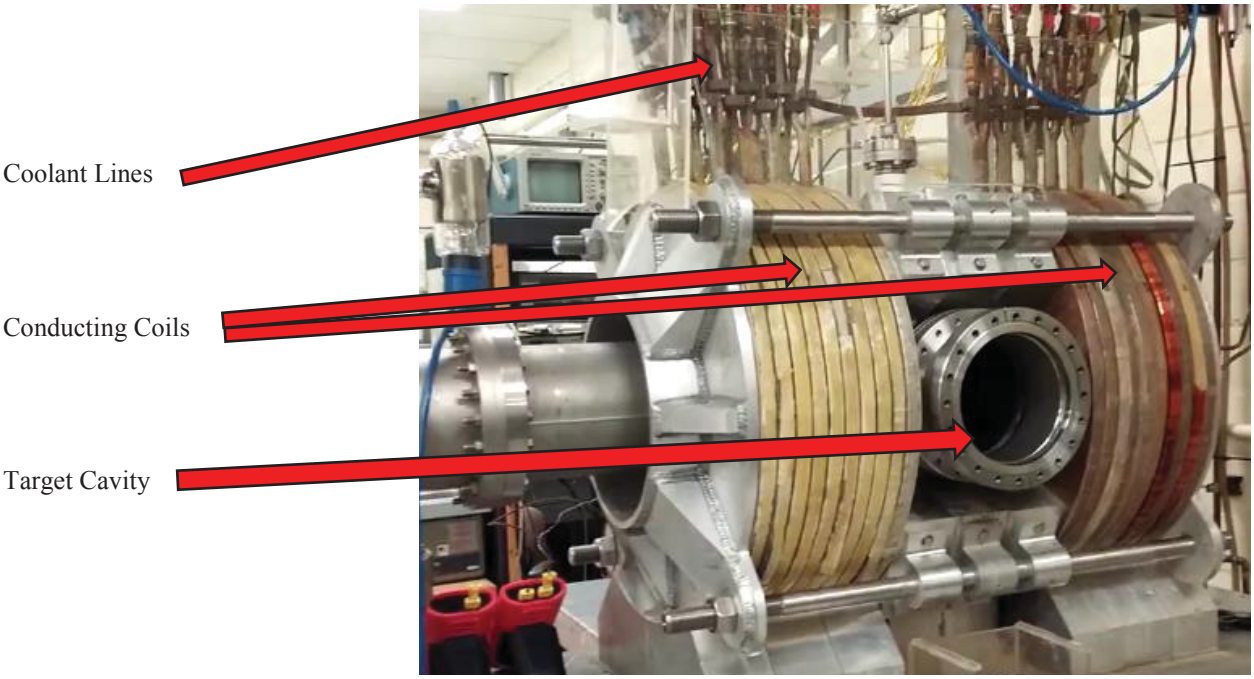

Figure 4: The Atomic Oxygen Facility at NASA Marshall Space Flight Center

Previously, only small material samples had been placed within the AOF. All exterior-facing cavities of the AOF terminate in standard 8 inch conflat flanges (CF). Measurements of the AOF dimensions shown below in Figure 5 provide a sense of scale in comparison with the 4 inch length and 2.0915 inch width needed to house the REDD device.

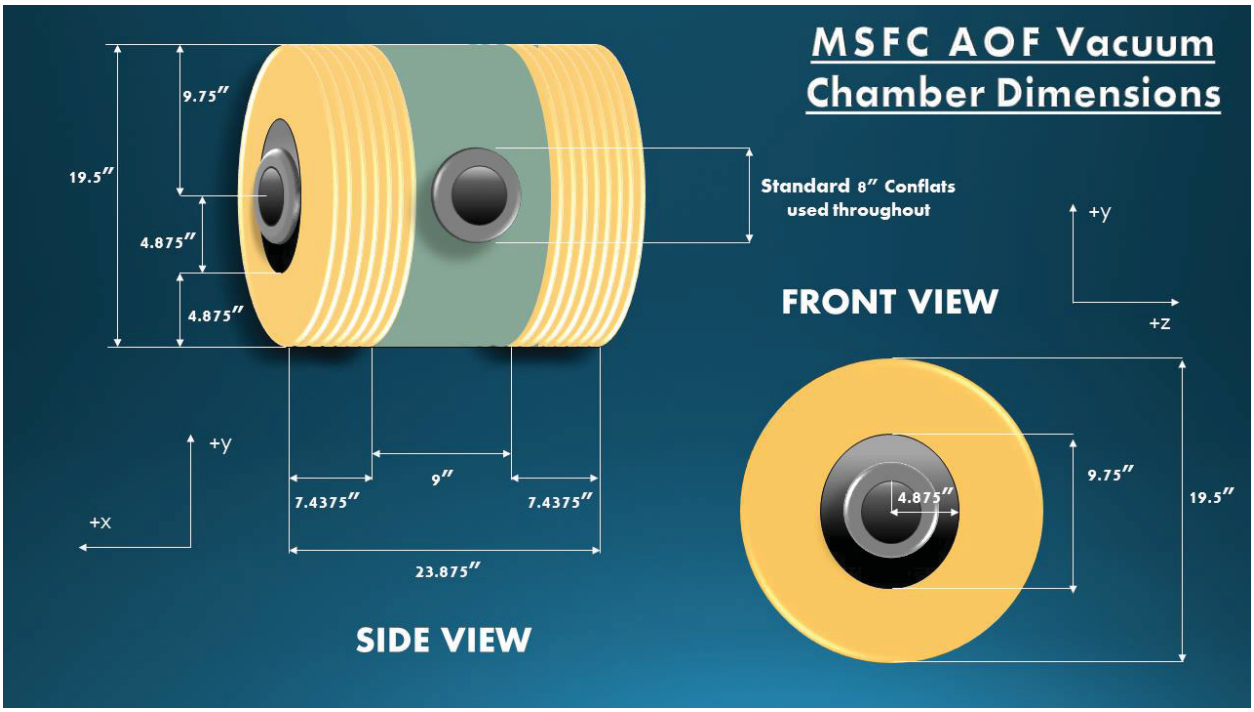

Figure 5: AOF dimensions: side and front views of the AOF with associated axes.

Magnetic Field Profile of the AOF

In order to utilize the AOF at MSFC for validation testing of the REDD instrument it is necessary to know the magnetic field geometry and magnitude within the testing chamber. The peak value of the magnetic field at the center of the chamber is known to be ~4 kG (Cuthbertson, et al., 1991). The field is expected to be solenoidal because it is produced by a symmetric coil system along the cylindrical axis of the vacuum chamber. A 4 kG field will have significant effects on the paths of the electrons emitted by the filament and on the trajectories of ions traveling through the device. The expected current output of the MCP is in the nA - μA range (Earle, 2016), and the pertubations caused by the magnetic field would render current measurements unreliable under these conditions. Validation testing in this environment therefore requires magnetic shielding at the location of a minimum in the solenoidal magnetic field.

A Lakeshore Model 460 kilogauss meter with a 3-axis transverse probe is used to provide accurate measurements of all three magnetic field components simultaneously. The meter provides a calculated magnitude as well. According to the datasheet, the Model 460 Hall effect gaussmeter is able to measure fields of 300 mG – 300 kG at an overall rated DC accuracy of 0.1% of reading. The 2.125 inch MMZ-2502-UH probe is utilized for its 30 kG range with an accuracy of 0.25% at 25° C with 5 digits of precision. The probe was calibrated using the included Lakeshore zero-gauss block. The magnitude of the Earth ambient field at room temperature within the MSFC laboratory containing the AOF has been previously measured to be 0.4-0.5 G, which was verified by the Model 460 reading of 0.412 G after calibration.

In order to map the field within the AOF with precision, it was necessary to stabilize the probe during measurement using a system resistant to magnetic force. Initially a non-ferrous aluminum stand was designed and fabricated at MSFC to enable measurement of the magnetic field radially outward from the neutralizer plate at the center of the chamber. As shown in Figure 6 two vertical rods supported an aluminum block, accommodating a sliding horizontal rod to which the probe was attached using Kapton tape. The stand could be manually adjusted using set screws to allow vertical adjustment of the probe arm height with respect to the table and horizontal adjustment in the Z direction into the target cavity of the AOF. Beginning in the center of the chamber, measurements taken at 0.5 inch increments as the probe moved radially outward revealed large field gradients that did not adequately resolve the field shape. Manual adjustment of the stand caused long-standing vibration of the probe arm due to the flexibility of the quarter-inch aluminum rods. Vibration of the probe in the strong DC magnetic field caused variations in measurement by an order of magnitude. Dampening the probe arm with sufficient counterweight to overcome oscillation of the probe tip would introduce permanent bending in

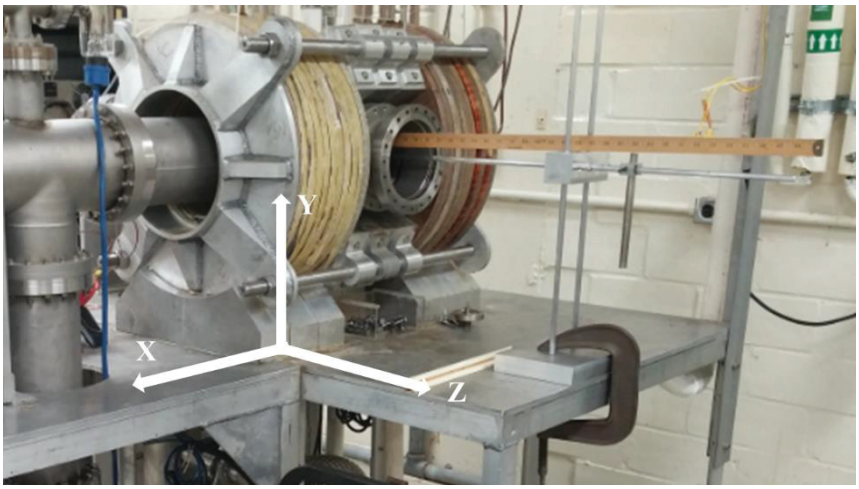

Figure 6: Original fabricated stand shows the original manually adjusted setup for the kilogauss meter probe

the rods due to the flexibility of aluminum. The need for greater stability and finer resolution led

to the construction and use of the stand in Figure 7 with the assistance of facility operator, Curtis Bahr. The new rigid stand increases stability significantly and allows for refined adjustment of the probe location with three degrees of freedom and 0.0625 inch resolution. A rail allows for smooth linear movement in the z-direction, but is limited to 15 inches radially outward from the neutralizer plate at the center of the AOF's vacuum chamber. The new design retains the non-ferrous quarter-inch aluminum rod to which the probe is mounted.

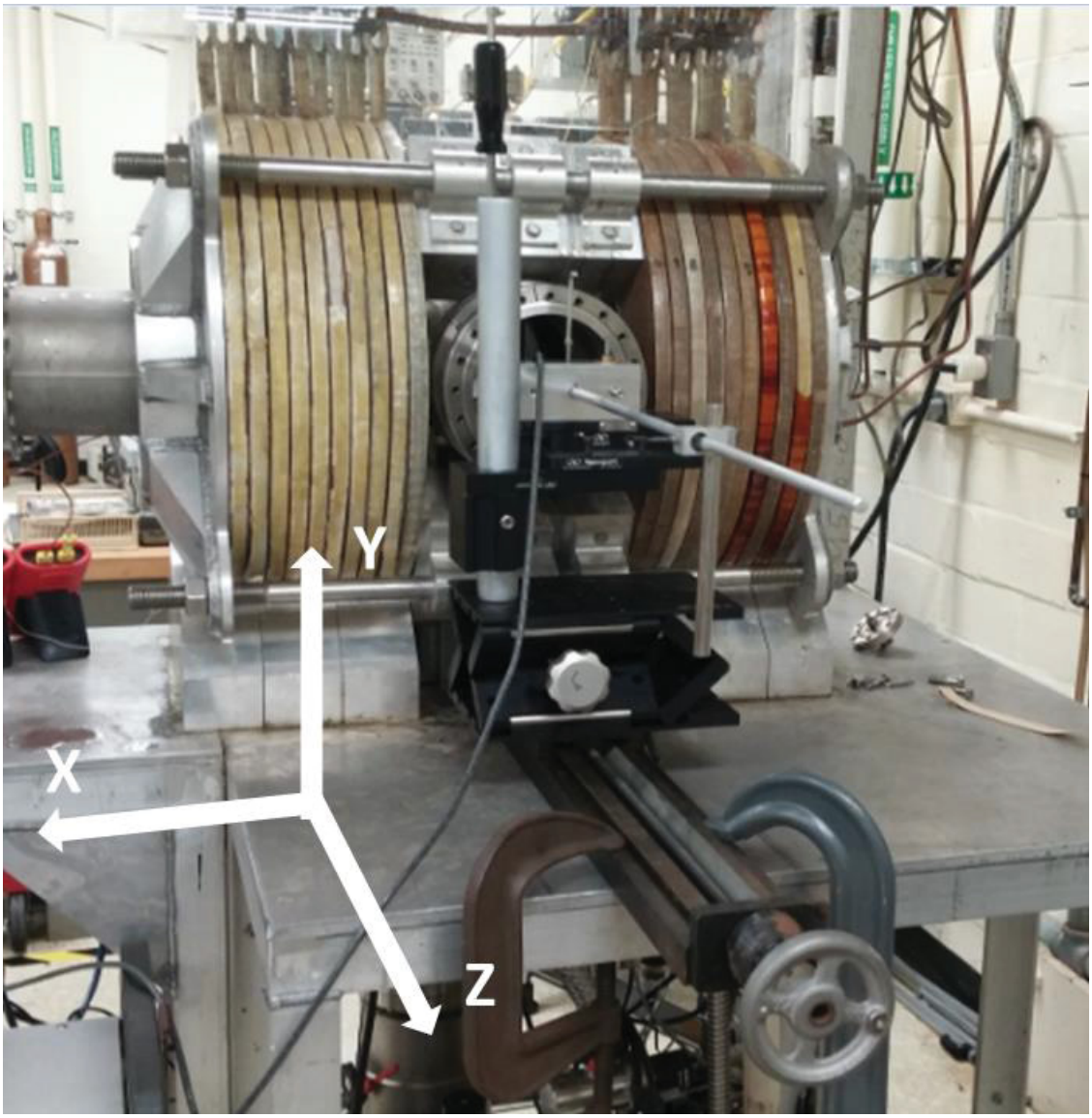

Figure 7: Updated probe stand allowing for increased stability and movement with three degrees of freedom

Location of probe measurements of the AOF magnetic field vector components and magnitude are taken with respect to the chamber center where the field magnitude has been previously verified (Vaughn et al., 1991). Orientation of the transverse probe and its associated measurement axes are shown in Figure 8. The X-axis is aligned with the AO beam's direction of

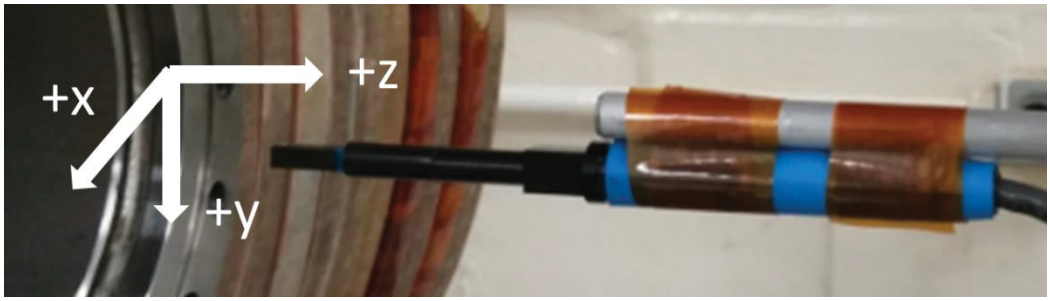

Figure 8: 3-axis MMZ-2502-UH probe, with XYZ axis orientation

travel and coincides with the longitudinal X axis of the coils, while Y and Z axis respectively coincide with transverse axes. Initial measurements in Table 4.1 show that the field magnitude at the location of the neutralizer plate is accurate in comparison to previous measurements considering ambient temperature of the coils and aging of the system (personal communication, Curtis Bahr).

Table 4.1: Initial measured magnetic field measurements within the AOF.

Measured Field at AOF Center	**X**	**Y**	**Z**	**XYZ Magnitude**
Ambient Field	0.144 G	0.216 G	0.320 G	0.412 G
AOF field activated	3.342 kG	151.14 G	110.19 G	3.347 kG

To locate a local minimum and establish a detailed profile both the shape and magnitude of the field are desired. Further in-situ field measurements were taken at the target cavity, extending 15 inches radially outward from center in increments of 0.25 inches (in the Z direction). Each trial

consists of five sets of radial measurements as shown in Figure 9: centered within the target cavity and aligned with the axis of the AO beam, ±1 inch in the Y-direction, and ±1 inch in the X-direction. The XYZ location with respect to the center of the AOF was recorded with each measurement, along with the respective component and magnitude values. The magnetic flux

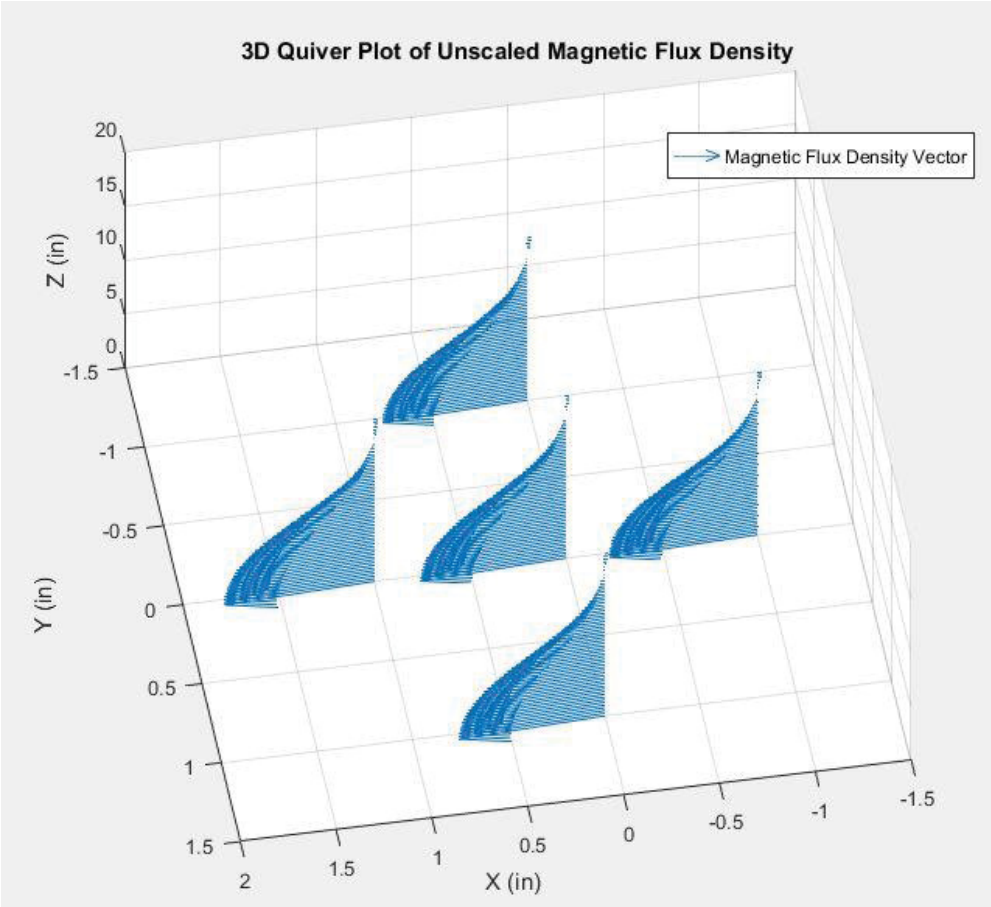

Figure 9: Unscaled 3D plot of magnetic flux density within the AOF target cavity. The relative length of the magnetic flux density vectors indicate the magnitude of the field strength. Each set of vectors represents measurements taken radially outward from the AOF center along the transverse Z axis during five separate trials centered at different positions.

density depicted at each increment in Figure 9 is depicted as a vector that points primarily in the x-direction with a length proportional to the vector magnitude calculated by the kilogauss meter. It should be noted that Bx, which lies along the cylindrical axis of the coils, dominates both the Y and Z components of the field for the large majority of the measurement trials. Nullifying this

X component of the magnetic flux density is identified as the main factor in mitigating any magnetic interference with the charged particles traveling within the REDD device.

These resulting measurement profiles were repeated and confirmed by the MSFC AOF technician in a separate trial. Each set of measurements confirm the existence of a null point in all three components of the magnetic flux density coinciding at the probe position shown in

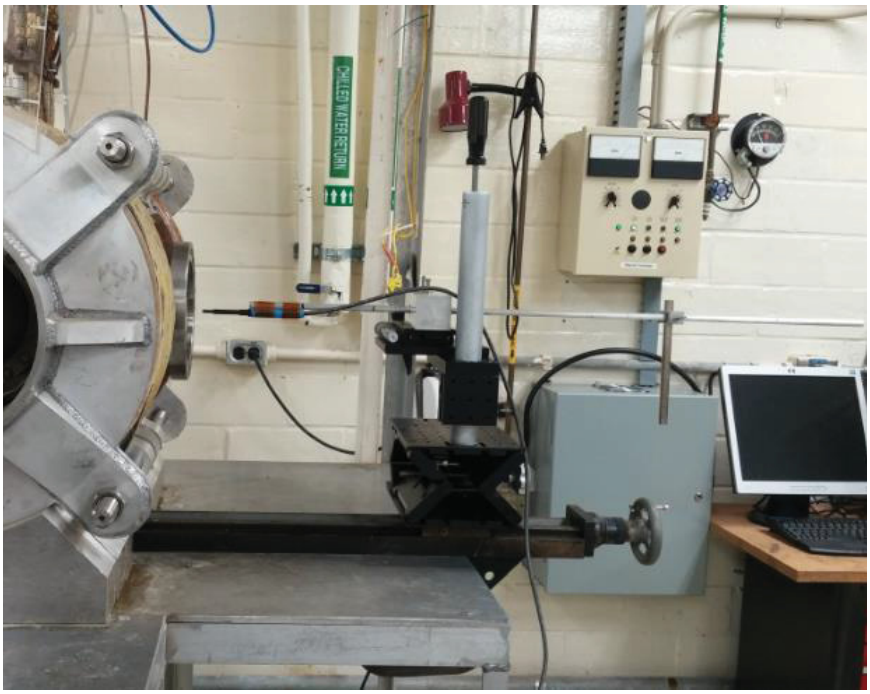

Figure 10: Location of a null point in all three components of the magnetic flux density.

Figure 10. This null point is located 13.25 inches radially outward in the Z direction and is centered on the X-Y axes relative to the chamber center. It resides in the area 1.25 inches outside the target cavity where the polarity of the field changes in the Bx and By components. Figure 11 shows a comparison of the respective 2D magnetic flux density plots and reveals a coinciding minimum for Bx, By, and Bz. Field strength in all three components of the magnetic field at this

location were measured to be at Earth ambient levels over a range of ~0.25 inches in the Z direction.

The measured values of magnetic flux density would have significant effects on the charged particles traveling through the REDD device. Particles moving perpendicular to a static magnetic field will move in circular orbits with a constant radius, called the Larmor radius. The form of Larmor radius used is given by the Equation (1) (Bittencourt 2013).

$$r_L = \frac{v_\perp}{\Omega_c} = \frac{m v_\perp}{|q|B} \qquad (1)$$

In order to minimize magnetic interference during the operation of REDD, the desired Larmor radius of charged particles traveling through the device should exceed 10-100 times the 9.403 cm length of the device. Table 4.2 illustrates the dominant effect of Bx, with magnitudes greater than 13.7 G causing charged particles to collide with the interior of the cylindrical sheath before reaching the MCP at the rear of the device.

Table 4.2: Calculated values for Larmor radius of an AO ion and ratio of instrument length to this Larmor radius at 293 Kelvin.

Bx	**R_L**	**Instrument Length / R_L**
0.5 G	25.87 m	275.12
1.37 G	9.44 m	100.4
13.7 G	94.43 cm	10.04
30 G	43.11 cm	4.59
300 G	4.31 cm	0.459

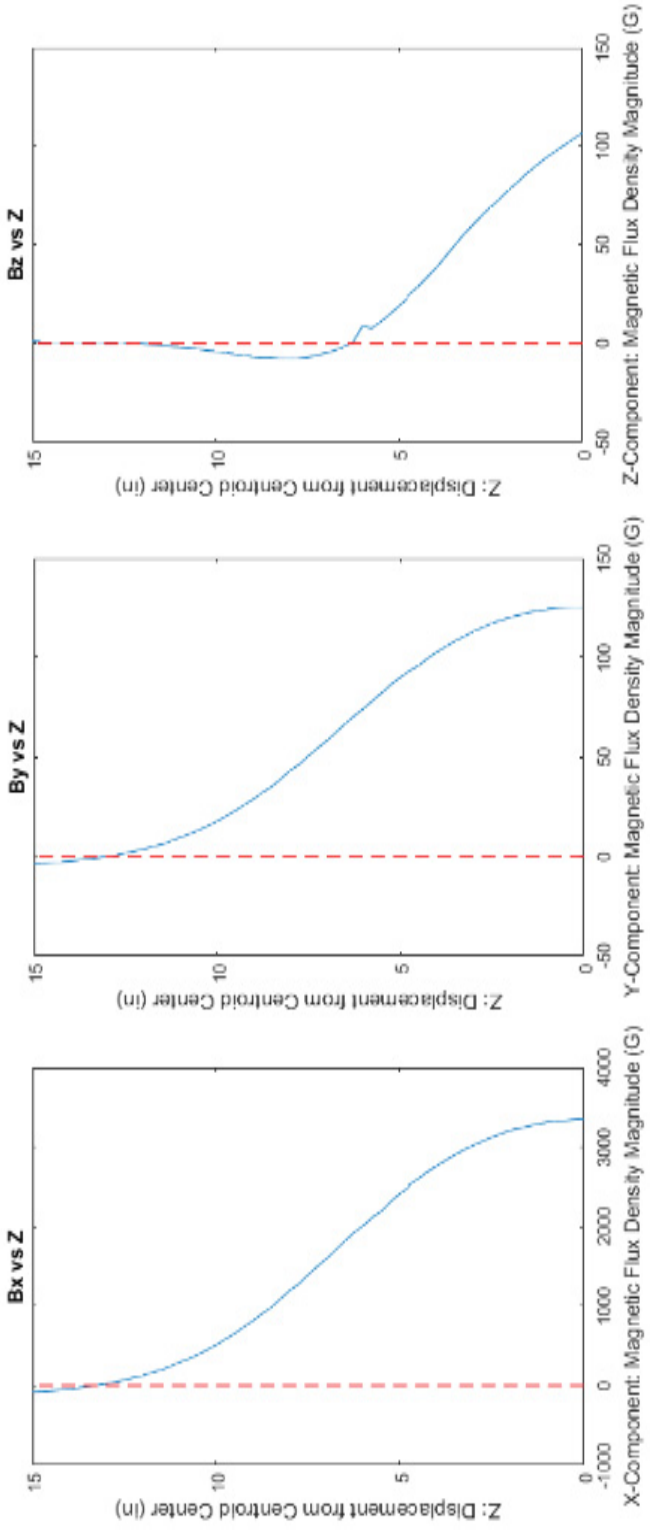

Figure 11-13: 2D plots of the magnetic flux density component profiles. Comparison shows a coinciding minimum occurring at approximately 13.25 inches from the origin.

The portion of the REDD device that is most sensitive to magnetic interference is the ~2 inch path travelled by AO ions from the ionization chamber to the MCP. Optimally, the minimum of the Bx and By components of the magnetic field should be located in this area. The change in polarity of the field after this null point in both the X and Y directions further ensures that charged particles do not collide with the interior walls of the device before reaching the MCP detector. Figures 15 and 16 depict this optimal location of REDD's most susceptible area within the magnetic field profile of the AOF from two respective viewpoints. In order to reduce the possibility of interference with the device, this sensitive area should be centered on the location of minimum magnetic flux density magnitude.

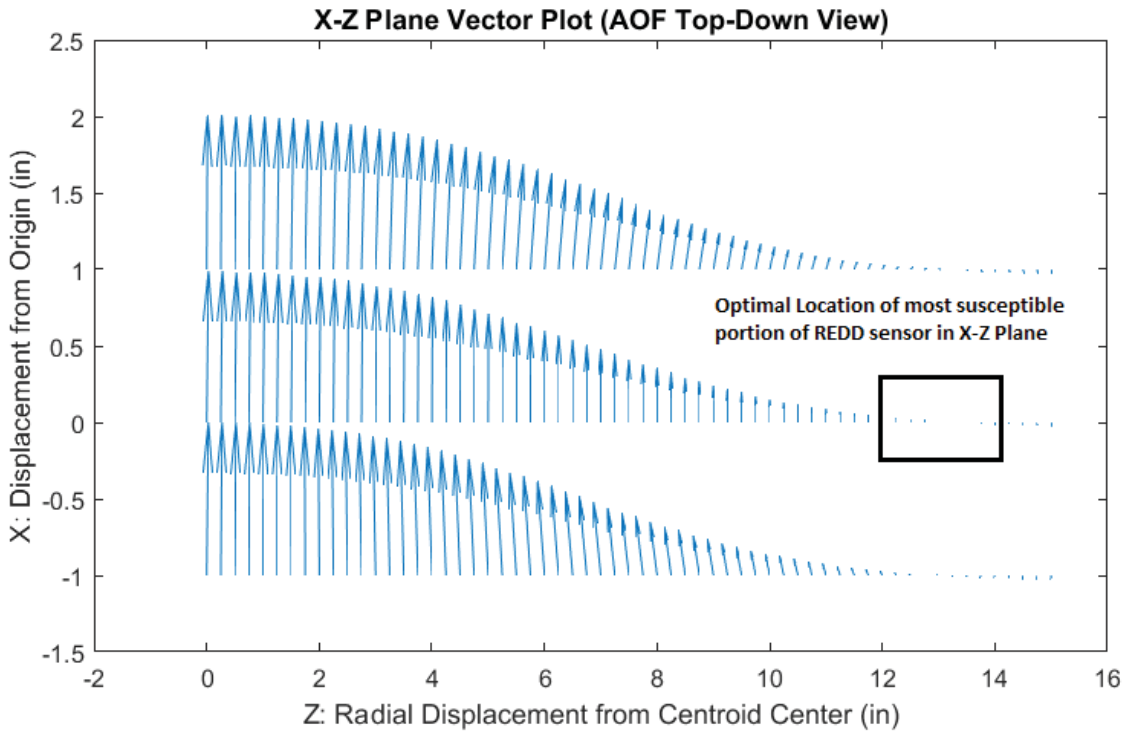

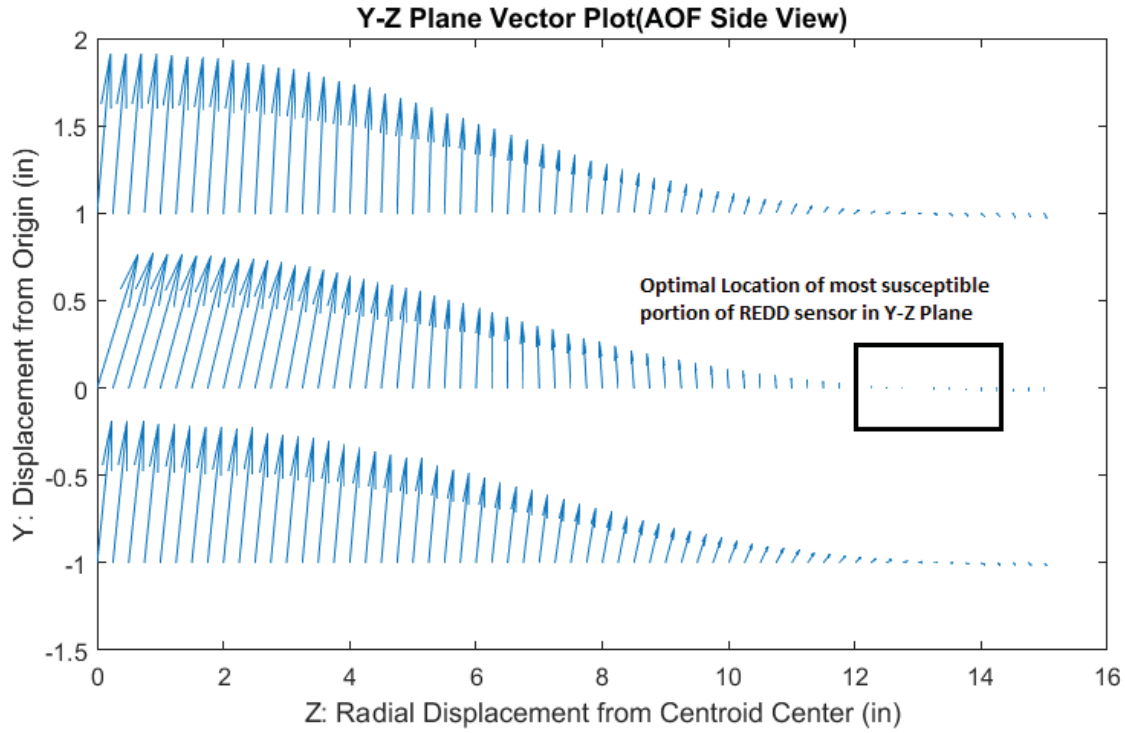

Figure 14a and 14b: Optimal location of the most susceptible portion of the REDD device within the magnetic field.

Methods, Software, & Apparatus

Hardware – Mount, Passive Shielding, and Interface

End-to-end testing of the REDD sensor in a relevant environment requires positioning the device with the aperture facing normal to the flow of the beam. Optimal placement of the device is aligned with the center of the beam that flows radially outward from the center of the chamber. Though both the flux and fluence rates of the system are known to the highest degree of accuracy at this location in the center of the chamber, REDD cannot be placed there as doing so would result in the very highest levels of magnetic interference. As previously stated, accurate and adjustable positioning of REDD is vital to testing the sensor within the AOF's intense magnetic field. In addition, μ-metal sheets are used to attenuate the field. Mounting the sensor at the location of the null point 13.25 inches from the chamber center requires modification of the system through the addition of a 12 inch extension in the radial direction, as this position lies

Figure 15: Custom REDD Mount: Magnetically isolated mounting system for positioning and testing of the REDD sensor attaches to the standard 8" CF.

outside the original target cavity as seen in Figure 16. Probe measurements were repeated to

Figure 16: Addition of the 12 inch chamber extension to the AOF chamber. Magnetic field measurements along the beam's axis were repeated to ensure the integrity of the field geometry and magnitude.

confirm this alteration to the chamber did not cause any significant changes to the magnetic geometry or magnitude of the field profile.

The interior surface of the standard 8 inch CF acts as a base, anchoring two aluminum guide rods 12 inches in length that extend into the target cavity. Magnetic isolation of the sensor

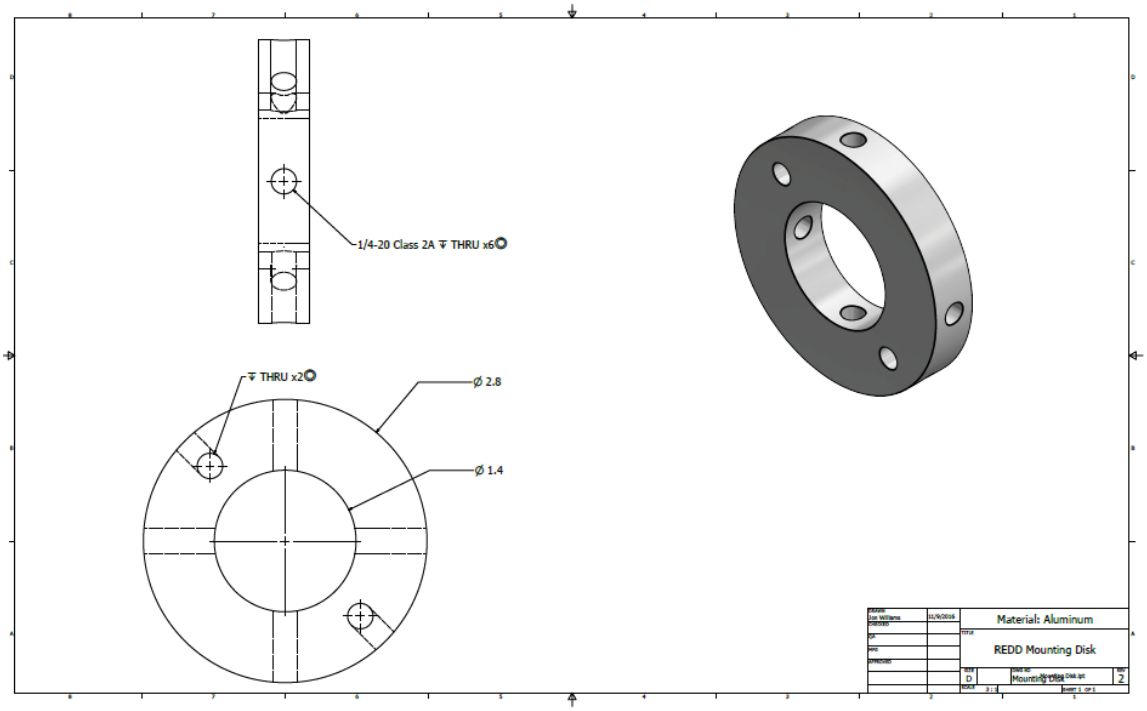

Figure 17: REDD Mounting disk drawing: Autodesk Inventor designed drawing of mounting disks

necessitated the design of the aluminum REDD mounting disk as seen in the technical drawing in Figure 17. This mounting disk was designed using Autodesk Inventor, and a pair were fabricated according to the specifications by MSFC personnel. Two quarter-inch through holes allow for linear adjustment along the guide rods parallel to the direction of the beam. The six tapped through-holes are intended to house two set screws to secure each mounting disk to the

guide rods and four to house nylon set screws for securing the sensor within the interior of the disks. The configuration is shown in Figures 18a and 18b. These nylon screws allow for stabilization and accurate alignment of REDD with the beam's angle of arrival while providing

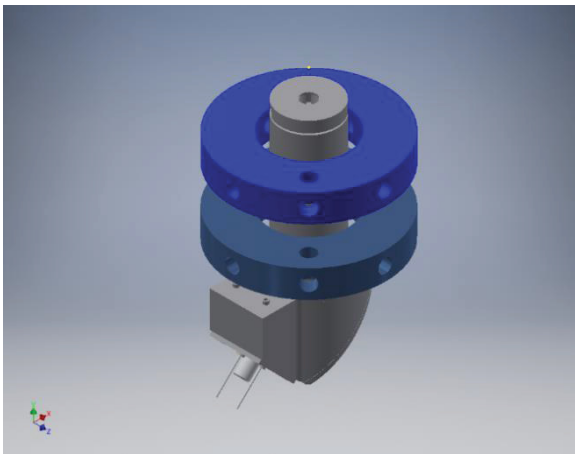

Figure 18a: Off-axis view of REDD mounting disk Autodesk Inventor 3D CAD model. Scale REDD sensor situated at the intended position within the disks for reference.

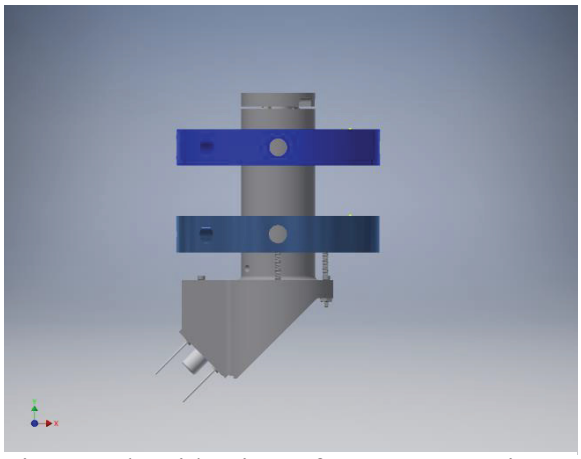

Figure 18b: Side view of REDD mounting disk Autodesk Inventor 3D CAD model. Scale REDD sensor situated at the intended position within the disks for reference.

the necessary magnetic isolation of the device from the aluminum disks and guide rods. Four

cavities extending through the CF base provide access to the needed connectors for operating and monitoring the REDD sensor.

Passive Magnetic Shielding

The main feature of the mount is the passive shielding system consisting of two concentric cylinders of μ-metal encasing the REDD sensor that are used to attenuate the field at this position and shield the device. The use of multiple shielding layers is due to the difficultly in reaching high shielding factors without reaching magnetic saturation in a single layer (Mager, 1970). Equation (1) was used to test the hypothesis that two concentric layers of shielding would be sufficient to suppress field magnitudes to approximately Earth ambient levels at the location of the REDD sensor (Personal communications, Dr. Ahmad Safaai-Jazi).

$$B^{inside} = \frac{9\mu_r B_0}{(2\mu_r + 1)(\mu_r + 2) - 2(\mu_r - 1)^2(a/b)^3} \qquad (2)$$

Where μ_r is the approximate permeability of the μ-metal, B_0 is the maximum field to be attenuated, and a/b represents the wall thickness ratio of the shields used. Using an estimated 80,000 for the permeability, 4000 G as the maximum field, and thickness ratio of ~1 to represent thin shields, the calculated field value with two cylindrical shield layers was calculated to be 4.847 G. Field magnitudes of this level were shown to be sufficient using Table 4.1 Wrapping each cylindrical layer multiple times was theorized to decrease this value further and guarantee acceptable suppression of the magnetic field was achieved. The inner layer of shielding seen in in Figure 19a is prevented from magnetically contaminating the sensor chassis by a thin layer of

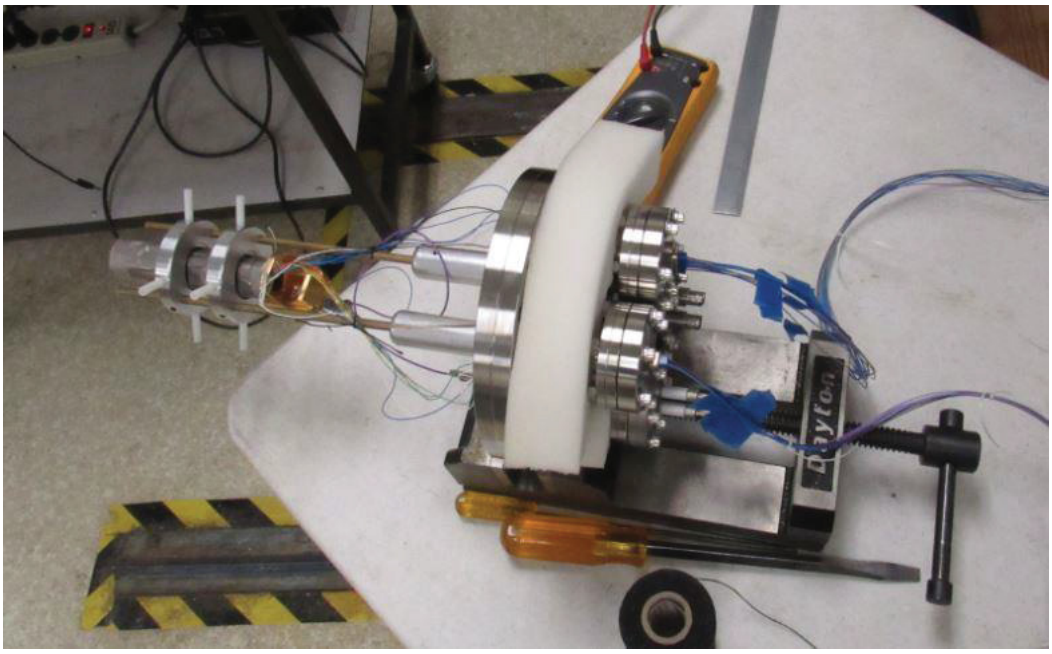

Figure 19a: Inner shielding layer wrapping the REDD sensor. The shielding is separated from the sensor sheath by a sheet of non-magnetically conductive Kapton.

non-conductive Kapton tape wrapped around the sensor. The outer shield is implemented by fitting the wrapped cylindrical shielding around the nylon set screws as seen in Figure 19b, and therefore preventing contact with REDD and magnetic contamination of the sensor. The μ-metal

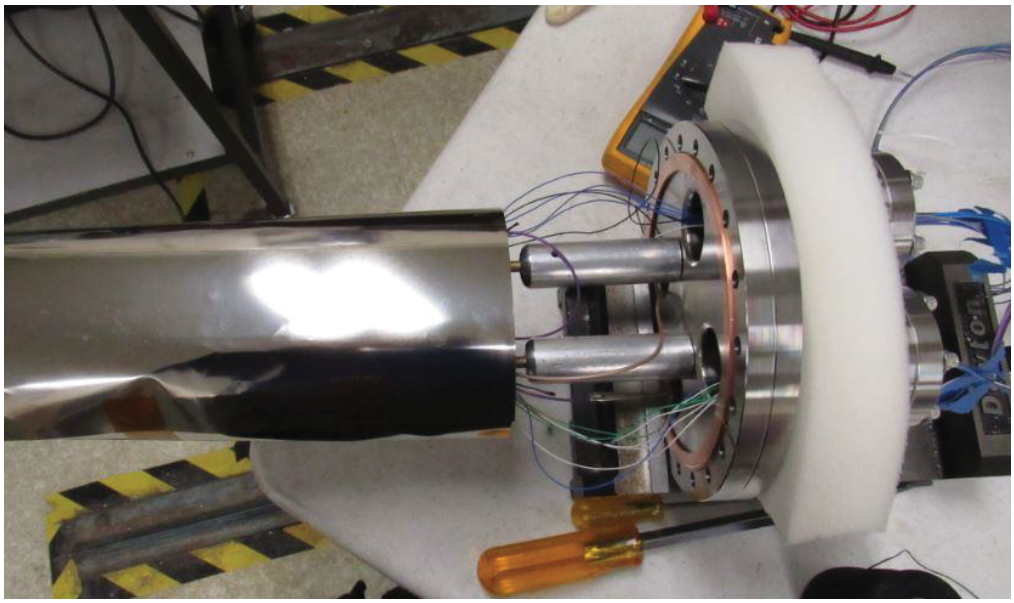

Figure 19b: Outer cylindrical shielding layer for the REDD sensor. Nylon set screws separate the shield from the REDD sensor and mount.

cylinders are left open at the endcaps to allow for exposure of the REDD aperture to the beam as shown in Figure 20. The unshielded Bz component of the field traveling in the on-axis beam direction has negligible effect on the ions traveling through the device. Leaving open the rear

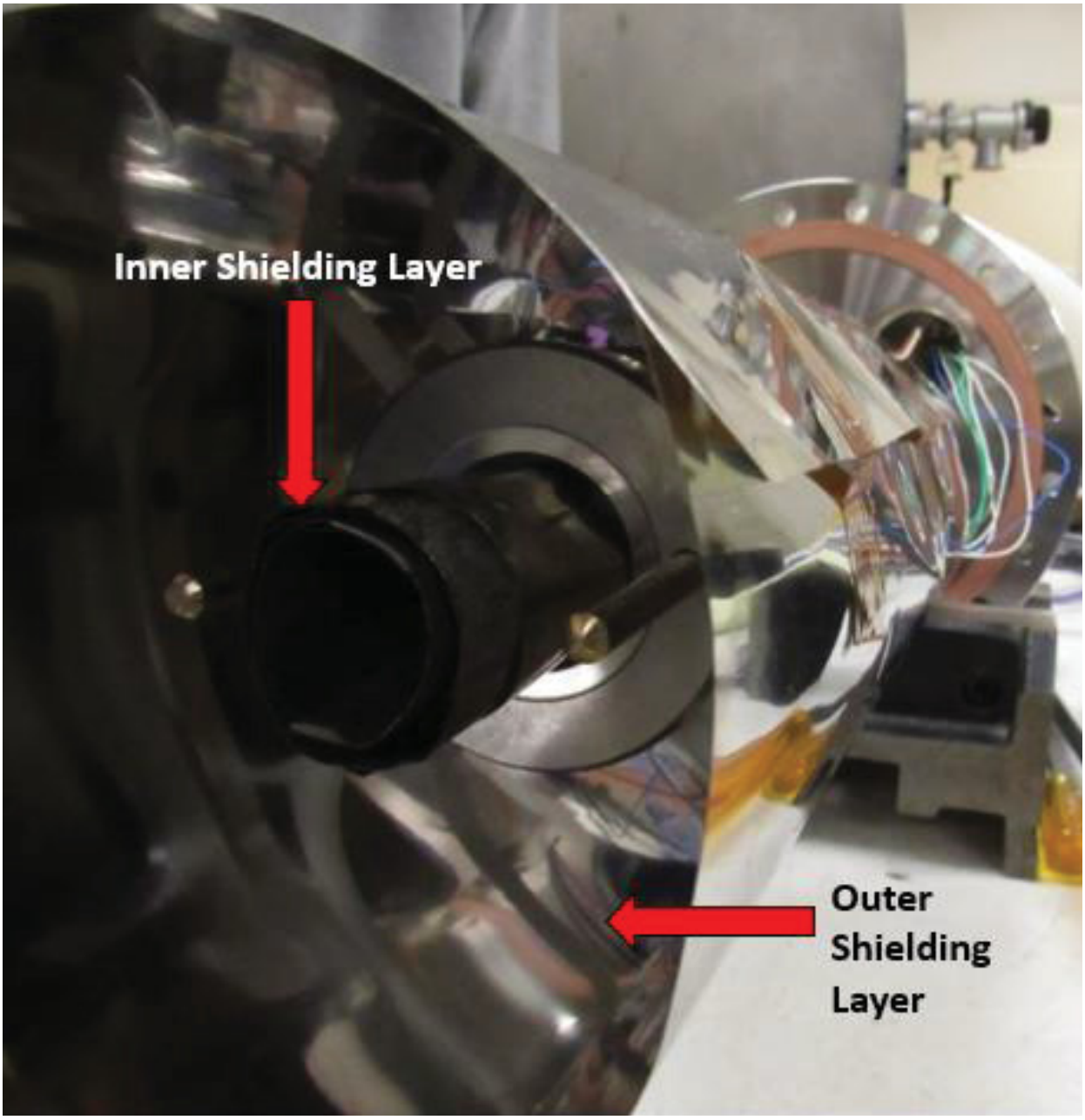

Figure 20: Front view of the passive shielding system for the REDD sensor. The inner and outer shielding layers are magnetically isolated from the sensor by the respective Kapton sheeting and nylon set screws that hold the device.

endcaps allows for the trailing wires to be threaded into four cavities leading to the respective vacuum-safe connectors.

Electrical Interface

These cavities terminate in four 2.75 inch CF's that house four distinct feedthroughs, as seen in Figure 21. This interface consists of two vacuum-safe DB-9 connectors, one BNC connector for

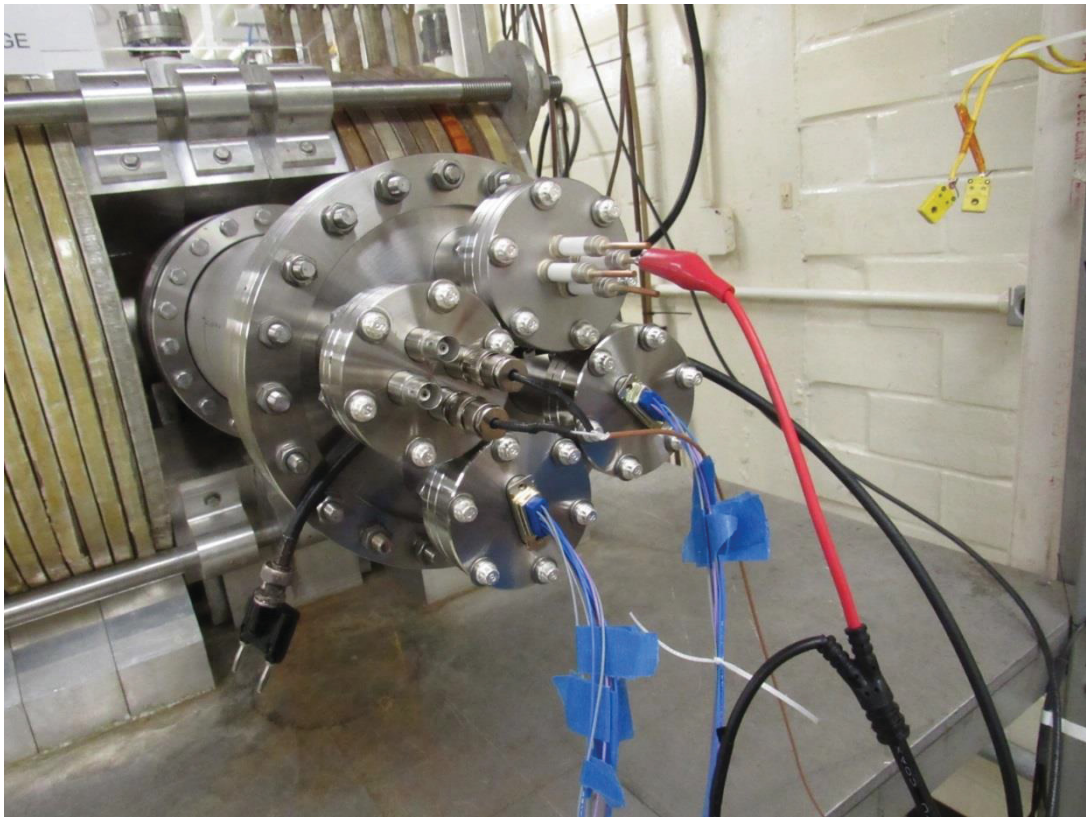

Figure 21: Rear view of REDD mounting system. Four feedthroughs allow for electrical interface between external equipment and the sensor inside the AOF chamber.

MCP output, and four available high voltage pins. The inclusion of additional connectors and added pins allows for alternate configurations and expansion of the electrical interface during future testing. The connectors above lead to the accompanying power supplies, two Keithley 6517b electrometers, and one Keithley 2000 to monitor temperature. A thermistor is attached to the ionization chamber within REDD using thermally-conductive paste to enable monitoring of

device temperature. Several material and geometry changes were made during construction and initial subsystem testing:

1. Tungsten filaments were formerly adopted as the source of electron production in the ionization chamber.
2. Step 1 facilitated the redesign and fabrication of backing plates responsible for mounting the filament and enclosing the ionization chamber sidewalls.
3. Aluminum brackets surrounding the ionization chamber were needed for additional heat sinking to mitigate the possibility of damage to the original Kel-F brackets.

Further electrical connection details concerning the interface, pin-outs, wire gauges, harnesses, and external equipment are detailed in the electrical ICD included in Appendix A. The Keithley measurement devices and power supplies necessary for sweeping the retarding grid voltages are controlled through a LabVIEW graphic user interface (GUI) developed for this purpose.

Software – REDD Testing GUI

To automate the test procedure a custom-designed GUI is needed since manual sampling of the 10 Hz AO beam with acceptable resolution is not feasible. The interface allows various empirical settings to be controlled, and provides feedback to the experimenters that can greatly improve the efficiency of validation testing. The LabVIEW programmed GUI detailed in this document is designed to provide a communication interface between the user, the REDD device, and the associated testing equipment. . The equipment communicates with the software using the IEEE-488 standard, otherwise known as General Purpose Interface Bus (GPIB). This software takes user input parameters and interprets the commands of controllable graphical elements in order to operate the Keithley 6517B, Keithley 2000, and Agilent 6645A. The software has

additional functionality that allows for real-time plotting of measurements and parsed data recording to an output file. The GUI was created and implemented using National Instruments LabVIEW, Versions 15 and 16.

The flowchart of the GUI seen in Figures 22 illustrates the path of data through the program beginning with initialization and ending with file output. The GUI is manually started, implements the chosen mode of operation, appropriately commands the external equipment, and displays the appropriate real-time information before recording data output. The program features flexible user control for a number of functions including choice of external equipment roles, mode select, plotting, output file location, and filename. The two modes of operation consist of a constant voltage mode for debugging and an automated sweep mode. The constant mode holds the retarding grid voltage at a single level in order to monitor current output, confirm capture of the pulse, and calibrate the system. The automated sweep mode holds the retarding grid voltage level for the desired amount of readings before increasing the voltage by user-specified increments. All data recording is handled by the script through a custom virtual instrument (VI) module that creates preformatted spreadsheets of the hardware settings and measurement device outputs in a native format compatible with a standard Microsoft Excel spreadsheet.

A view of the GUI front panel shown in Figure 23 showcases the various controls and displays available to the user. This Front End view of the LabVIEW software is intended to represent the GUI during normal operation while the hidden back end provides direct access to the modules,

configurations, virtual wiring, and the more technical coding. Prominent features of the front panel include:

- Input/output (I/O) initialization panel
- Manual start and stop buttons
- I-V control panel with mode select
- Real-time displays of temperature, voltage, iteration, current, and plots
- Sample controls for batches and plots
- Initial value cluster panel for data record management

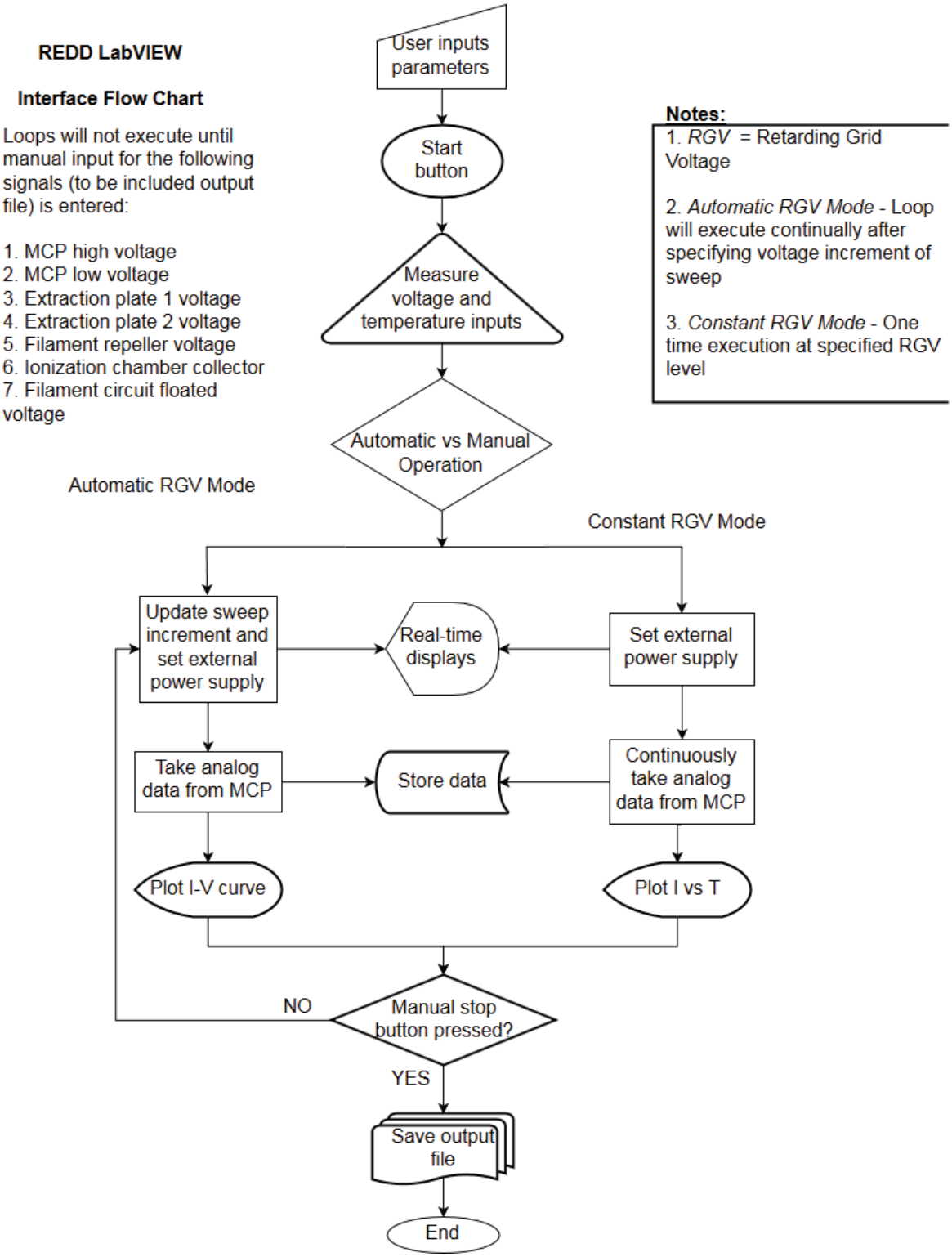

Figure 22: Flowchart showing dataflow for the LabVIEW Graphic User Interface (GUI). The GUI automates data collection for the REDD sensor.

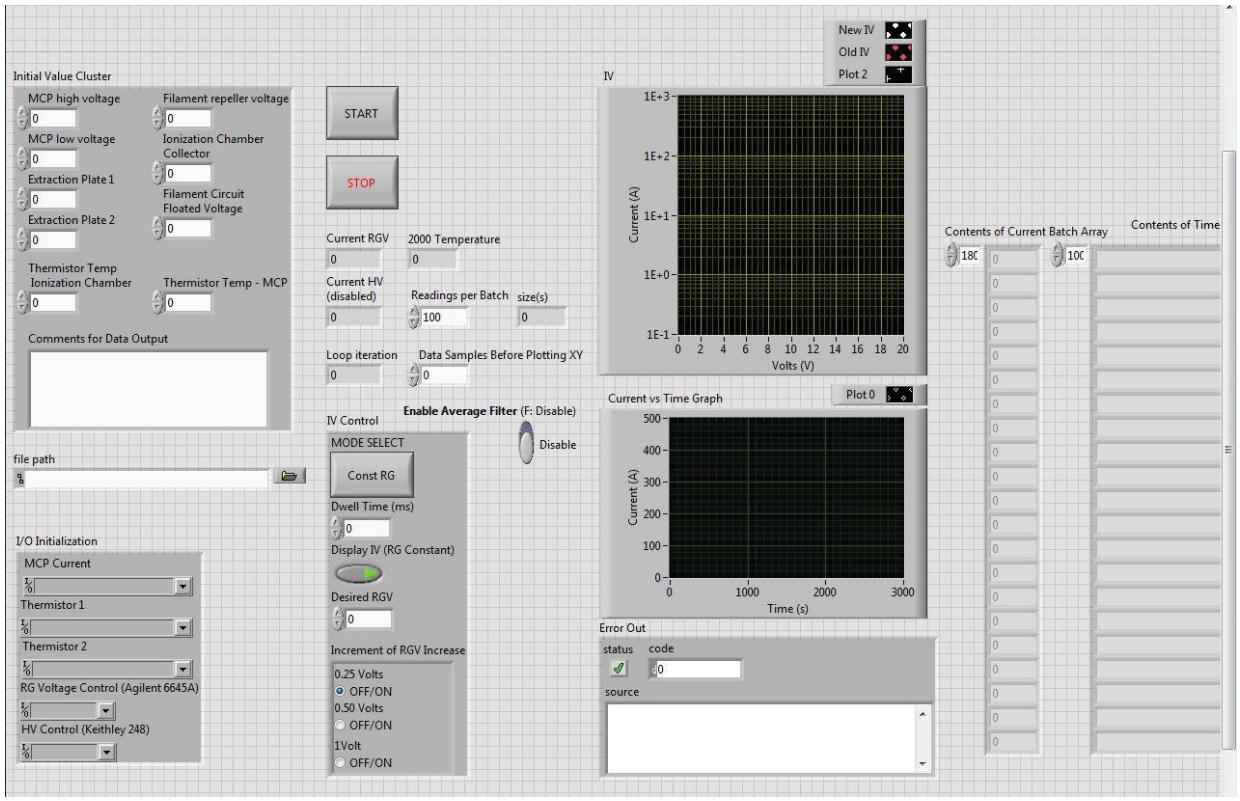

Figure 23: REDD GUI Front Panel View: The front panel of the GUI takes user-entered input parameters and automates the test procedure. The various indicators display real-time readings of device temperature, retarding voltage level, iteration, and current readings, while plotting output data. User-operated manual buttons include the Start, Stop, Mode Select, Display IV, and Enable Average Filter.

The I/O Initialization panel features drop-down dialog boxes that allow for flexible instrument choice. The program is currently configured to utilize the Keithley 6517b for MCP current measurement, Keithley 2000 for temperature measurement, and Agilent 6645A for voltage control. These panel features are extended for the optional addition of other instruments, including HV Control for automation of the Keithley 248 HV Supply and an additional Keithley 2000 or 6517 for monitoring a second thermistor.

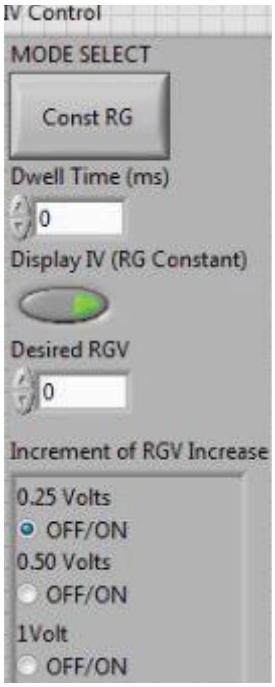

Figure 24: Front panel REDD IV control panel. Features an interactive Mode Select button and a Display IV button that visually indicate their current status. User-specified Dwell Time and Desired RGV are used in the Constant RG mode. Auto RG Mode utilizes radio button controls for the desired Increment of RGV Increase.

Figure 24 shows the IV Control panel features. The "Mode Select" button features the currently selected mode of operation on its face and uses the lower controls appropriately based on the choices selected prior to manually starting the program. "Const RG" displayed on the button represents the constant retarding grid mode, in which the retarding grid voltage is held at a set level specified by the "Desired RGV" user control. The "Dwell Time (ms)" control limits the time period of measurement defined by the millisecond value entered by the user, while a value of 0 allows batch measurements to continue indefinitely. Pressing the Mode Select button changes the displayed button text to "Auto RG" to represent operation of the GUI in sweep mode. In this mode the program utilizes the "Increment of RGV Increase" choice selected by the user prior the program start. This increment function is implemented using a case selector in

LabVIEW based upon the diagram shown in Figure 25. Retarding grid voltage level changes occur after each complete batch of current measurements is taken.

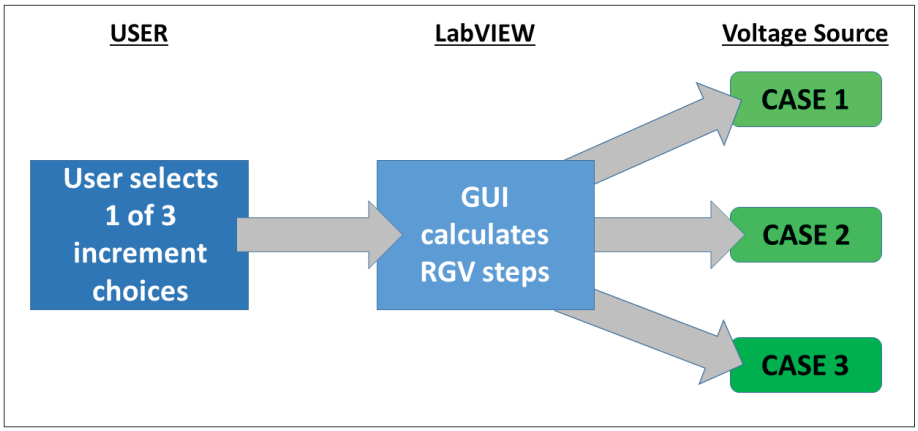

Figure 25: Case selector block diagram. The user chooses from one of three cases. The GUI calculates the necessary voltages to be applied by the external power supply for each case.

The number of current measurement samples collected per batch by the Keithley 6517b is controlled by the "Readings per Batch" field utilized in both modes of operation. This control's description is listed in Table 5.1 among the available real-time displays.

Table 5.1: Real-time displays and their associated descriptions.

LABEL	DESCRIPTION
Current RGV	The current retarding grid voltage (RGV) bias as seen by the RG Voltage Control instrument.
2000 Temperature	The temperature (°C) reading calculated during the preceding RGV check using the Thermistor 1 instrument reading.
Current HV	The current high voltage (HV) bias as seen by the HV Control instrument.
Readings Per Batch	User-specified control to determining the number of concurrent measurements to be taken by the MCP Current instrument.
Loop Iteration	The current loop iteration (Const RG Mode) or sweep iteration (Auto RG Mode).
Data Samples Before Plotting XY	User-specified control determining the number of concurrent data samples passed to the plotting VI's.

Batch size and loop iteration are included for debugging purposes to ensure that correctly sized arrays for measurement batches were created by the program at each iteration. The "Data Samples Before Plotting XY" control allows for increased GUI performance by limiting point drawing within the respective plots to occur in batches. This is a necessary addition as lines drawn using point-at-a-time plotting during 1000 point batches proved particularly taxing on the GUI's sample rate. The LabVIEW built-in sub-VI operating the real-time plot windows forces a new bitmap drawing to the display after each update, slowing batch measurement sample rates by two thirds in the initial 1000 point batch test. This was overcome by using the Data Samples Before Plotting XY control to limit the amount of plot updates to user-specified intervals. Further testing revealed values ranging from a minimum of 10 points to a maximum of the Readings per Batch value selected by the user. This approach allows for smooth plot formation with negligible latency.

Monitoring the temperature of the ionization chamber is critical to enabling validation of the REDD sensor. This chamber houses components supplied with 2 amps of current, which is necessary for a filament based ionization source. The hot filament that sources the ionizing electrons poses a risk to non-metallic components in close proximity to the filament. Various Kel-F components within the device may experience outgassing at temperatures above 90°C, and the MCP may incur damage or produce inconsistent measurements as a result. The temperature is monitored by converting the measured variable resistance value of the Honeywell 10K NTC thermistor into the corresponding temperature. The conversion varies per resistor and the temperature range of interest. Calibration uses the Steinhart-Hart polynomial coefficients to

determine the actual device temperature (Steinhart, Hart, 1968). This is achieved by calculating three coefficients, beginning with the A and B coefficient approximations seen in Equations (3) and (4) and using T_0 = 298.15 Kelvin = 25°C and its related $R_0 = 10\text{K}$ and $\beta = 3974$ values, which are provided by the NTC 10K thermistor datasheet for calibration.

$$A = \left(\frac{1}{T_0}\right) - \left(\frac{1}{\beta}\right)\ln(R_0) \qquad (3)$$

$$B = \left(\frac{1}{\beta}\right) \qquad (4)$$

The C coefficient is initially approximated as 0 for estimation purposes. This allows for calculation of R_1 for a respective temperature T_1 in the desired range using the A, B, and C coefficients above within Equation (5) below.

$$\frac{1}{T} = \text{A} + \text{B}\ln R \ + \ \text{C}\,(\ln R)^3 \qquad (5)$$

Alternately, rearranging the Beta Parameter Equation (6) and solving for variable resistance R_2 yields Equation (7).

$$\beta = \left(\frac{T_2 T_1}{T_2 - T_1}\right)\ln\left(\frac{R_1}{R_2}\right) \qquad (6)$$

$$R_2 = \left(\frac{R_1}{e^{\left[\beta\left({}^{T_2 - T_1}/_{T_2 T_1}\right)\right]}}\right)\ln\left(\frac{R_1}{R_2}\right) \qquad (7)$$

After substituting a desired T_2 in Kelvin, the prior equation can then be solved for R_2 to provide the expected resistance at a chosen temperature T_2 within the desired range of 0-100°C. This range is chosen to avoid possible outgassing effects of Kel-F components within the device

should they surpass 100°C. Further refinement is achieved by solving for the C coefficient specifically to achieve more accurate values. The refined values derived from Equation (5) were substituted into Equation (7) to provide resistances remarkably close to publically available Honeywell NTC Thermistor comparison charts as well as sample expected values found within the datasheet. Expected resistances were further confirmed empirically through comparison with lower-end measured temperatures near 25°C. Several expected resistances are calculated using datasheet approximated coefficients, then repeated using the method above and more accurate substituted values. Table 5.2 shows a slight refinement in accuracy through a comparison of the initial approximated coefficients versus refined calculated coefficients for the selected resistances and their corresponding temperatures.

Table 5.2: Comparison of Initial approximated coefficients vs calculator-modeled coefficients

Resistance (Ω)	Temp (°C)	Initial Approximated Coefficients	Calculated Coefficients
10,000	25	A = 1.03652e-3	A = 1.03636e-3
3879.73	48	B = 2.51603e-4	B = 2.5163e-4
3565.91	50		
1072.115	85	C = -0.594e-7	C = -6.709e-7

The temperature calculation occurs within the program, occurring simultaneously alongside other batch measurements using a custom designed sub-VI, “Thermistor Resistance to Temperature (Steinhart-Hart Model).” This sub-VI is further explained in Appendix B.

Reliable data capture through the USB-connected GPIB required significant interface modifications to overcome issues related to rapid communication between the GUI and the

Keithley 6517b used for MCP current detection. According to the 6517b manual, the meter is ideally capable of recording low-current precision measurements at 400 samples/sec without the need for memory storage, and 125 samples/sec if applied to internal memory storage. Testing of the 6517b showed that the rate declines if the meter is forced to display information on the digital readout, or if the device performs any non-measurement functions. Furthermore, in order to transfer a measurement through the GPIB, the meter must cease taking measurements for a short time while sending information concerning the measurement, units, and current measurement range. These factors each introduce delays between measurements that severely limits the sample rate and disallows continuous acquisition of the 10 Hz pulse. This presents a significant obstacle toward utilizing the current testing system to adequately capture the pulse and validate the REDD device.

Overcoming this latency issue required several non-trivial modifications to early versions of the GUI including changes to the internal settings of the Keithley 6517b. The deployment of the "Trace Buffer" VI module specific to the 6517b allowed for batch measurements and user control over the number of measurements per batch. The Keithley 6517b is then able to record MCP output continuously over long periods while minimizing the amount of time spent reading query, status, parity bytes, and sending receive confirmations. By first recording measurements to the internal buffer, the VI grants the meter the capability to avoid communication delays inherent during each communication with the GUI. This change required advanced modifications to send native language commands through the 6517b Trace Buffer VI to the meter in order to accelerate the sample rate, suppress nonessential functions, and restrain the flow of extraneous data. These commands detailed further in Appendix B include significant alterations to buffer

size, buffer allocation, packet contents, filtering, readout display, measurement accuracy and resolution. In addition, this enhanced functionality is what allows for direct user interaction with the “Readings per Batch” and “Enable Average Filter” controls, as well the capability for back-end GUI access to the other parameters. The transfer of the internal buffer contents through the GPIB interface adds an additional delay proportional to the size of the batch measurement array, in the worst case introducing three seconds of delay in order to record batches of 1000 measurements. This delay is an acceptable cost for achieving the maximum 125 samples per second rate indicated in the device documentation. They less than 1.5 sec delay seen during batches of 500 has little effect on the sweep mode of operation because measurement is halted during changes to the retarding voltage, ensuring that the Agilent 6645A’s output current is given time to stabilize at each new setting.

Real-time plotting is available to the user through a simple interactive On/Off switch. This added functionality is provided in the event the user wishes to concede computing resources to other tasks and avoid the processor-intensive task of graphically displaying large data batches during normal operation, or for use on a slower computer. The two separate plotting windows seen previously in the top right of Figure 24 and detailed in Appendix B are reserved for displaying the respective I-V characteristics and current (I) vs time (T) plots. The upper window showing the I-V characteristic is able to display the relationship between MCP output current data and the retarding grid voltage as measurements are taken. Previous measurement batch results are held in a shift array. Holding this batch in memory allows for viewing of the previous trial overlaid by the current set of measurements as they are plotted being generated in real-time.

Real-time viewing of both the current and previous measurement batches allows immediate comparison of output data and enables identification of prominent features during the test. This is a very useful property, since it allows the user to quickly assess the impact of changes made to the settings of the REDD sensor. The scatter plot of current vs time automatically expands its time axis to match the amount of data collected. This plot grants the user the ability to more readily study electrical current output for a particular retarding voltage level over long periods of time. This also provides a valuable debugging tool to the user in identifying issues such as pressure changes, outgassing events, insufficient or widely varying emission currents, or particle energy fluctuations. Issues such as these were encountered during testing and were significantly easier to identify and mitigate by viewing the real-time plots of current vs time.

Data recording is handled by two modules within the GUI. Initial reference values, retarding grid voltages, temperature, and current output are automatically recorded and exported to LabVIEW's native Technical Data Management Structure (TDMS) format. This format is conveniently compatible with MS Excel and other standard spreadsheet viewers outside of the LabVIEW software environment. The Initial Value Cluster panel shown in the upper left of Figure 24 gives the user the ability to record relevant testing parameters to the output file including MCP voltages, extraction plate biases, starting thermistor temperatures, ionization chamber collector bias, filament floated voltage, and additional comments. This panel allows the user to easily record changes in control variables that are automatically written to a separate worksheet within the output data structure. These values are then handled by a custom subVI that converts these values to strings and creates a preformatted spreadsheet. The main fields of the spreadsheet are then populated with timestamp, temperature, retarding grid voltage, and MCP output values.

End-to-End Testing

Enabling validation of the REDD device requires vacuum end-to-end testing prior to delivery at NASA MSFC for final chamber testing. Prior testing of the electrical system was carried out by Adithya Venkatramanan and Lee Kordella. Subsystem testing of the device and validation of the GUI were carried out at Virginia Tech using the test setup shown in Figure 26. Static testing confirmed aliveness of the device and functionality of the software.

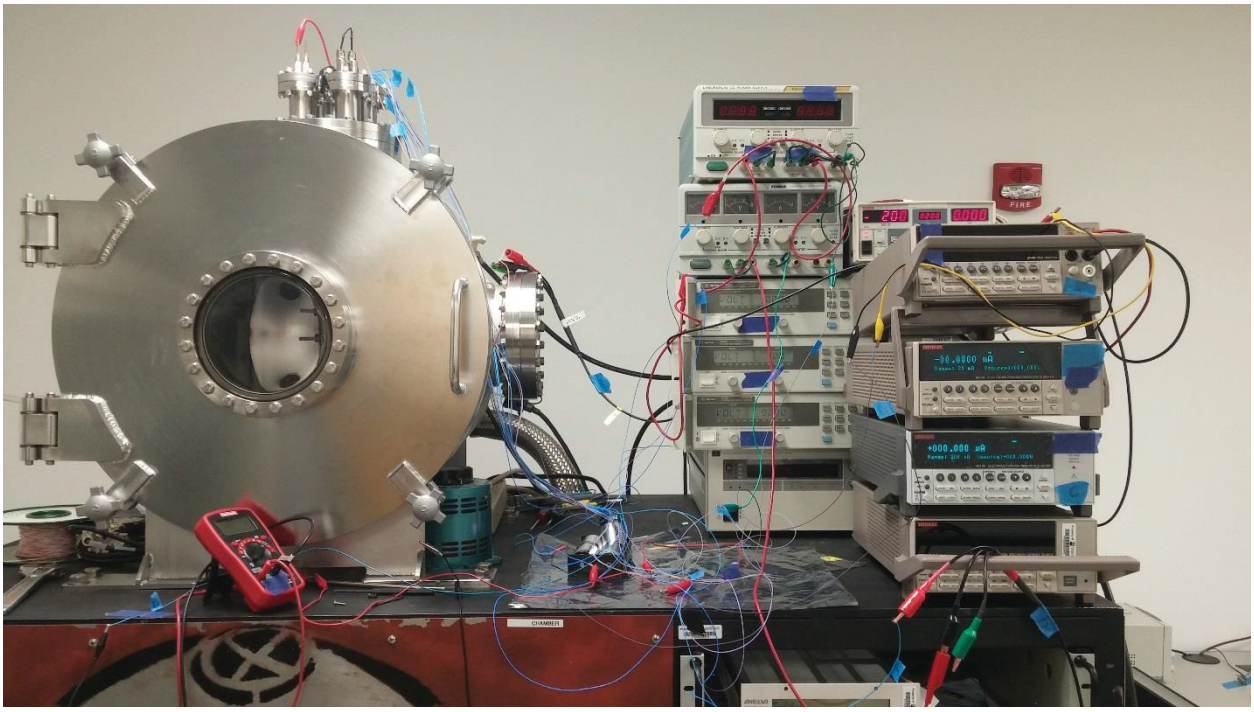

Figure 26: Vacuum chamber setup for initial aliveness testing conducted at Virginia Tech.

Several issues were identified and mitigated during the initial testing phase. For example, initial measurements showed a need for improved ionization efficiency due to the inconsistent performance of a commercial off the shelf part that produced the electron beam. As stated in the hardware section, this part was replaced by a tungsten filament to increase electron emission and

ionize a larger distribution of neutrals traveling through the aperture of the REDD sensor. COMSOL simulations such as Figure 27 suggest that biased tungsten filaments can provide sufficient electrons to ionize incoming neutrals. This figure depicts the particle trajectories of electrons created within the ionization chamber as they pass the -100V biased filament and travel toward the biased -100 V grid. The vertical line through the center of the model represents the incoming path of neutrals entering the device with an initial orbital velocity. The energetic electrons are emitted from the filament and ionize some of the neutral particles as they travel from the aperture toward the grid stack. Positive ions are produced in the resulting collisional interactions.

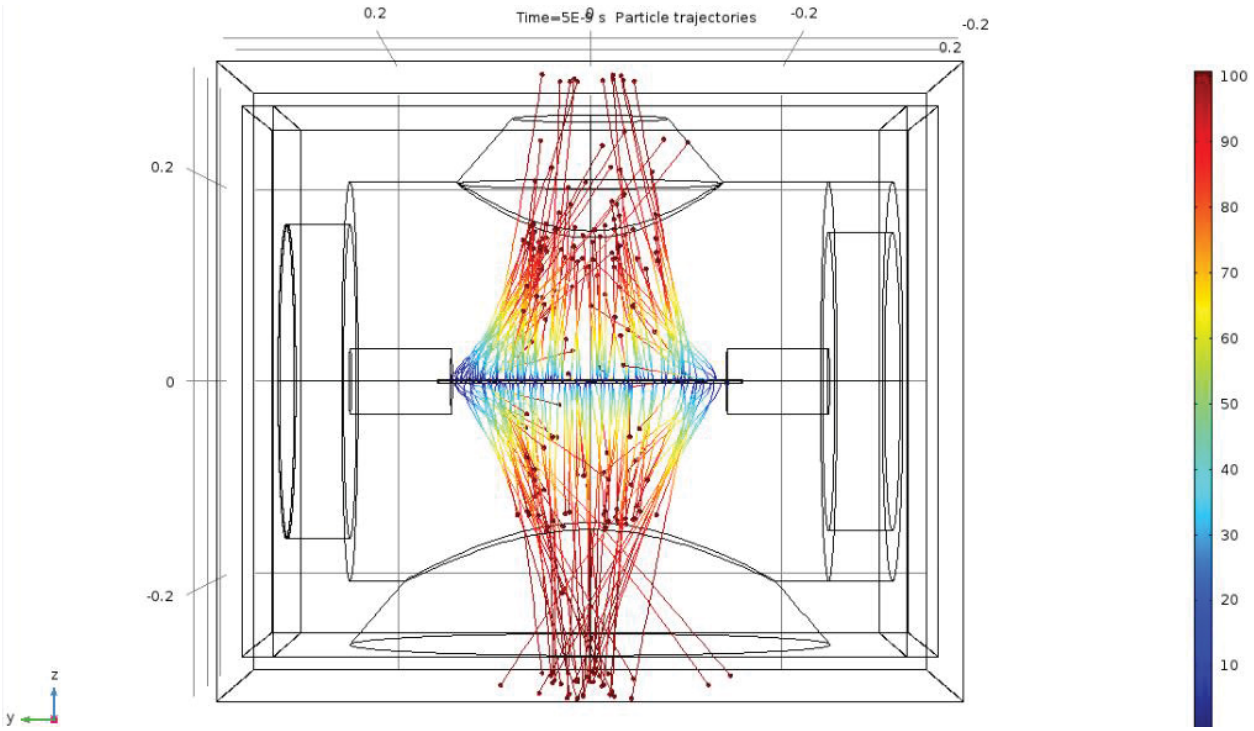

Figure 27: COMSOL simulation of estimated particle trajectories and their respective energies in electron volts (eV), as represented by the color scale situated on the far right. Ionization is most likely in the regions where electrons have greater than 90 eV of energy.

The geometry change more closely resembles the flight configuration of the C/NOFS RWS that utilized filaments as an electron source during its operation. In order to avoid rapid degradation

of the filaments used, a rudimentary current source powered by 4 D-cell batteries was provided by the AOF operator to enable ramping of the filament in-rush current. This proved a vital addition to the testing setup that decreased the frequency of filament replacement significantly. Preparation for each end-to-end testing of the REDD device is outlined below. The sensor was first attached to mount and associated magnetic shielding as detailed in the hardware portion of this document. The mount was installed to the AOF target cavity CF, oriented as seen in Figure 28 with REDD aligned in the on-axis direction of the beam. The chamber pressure was pumped

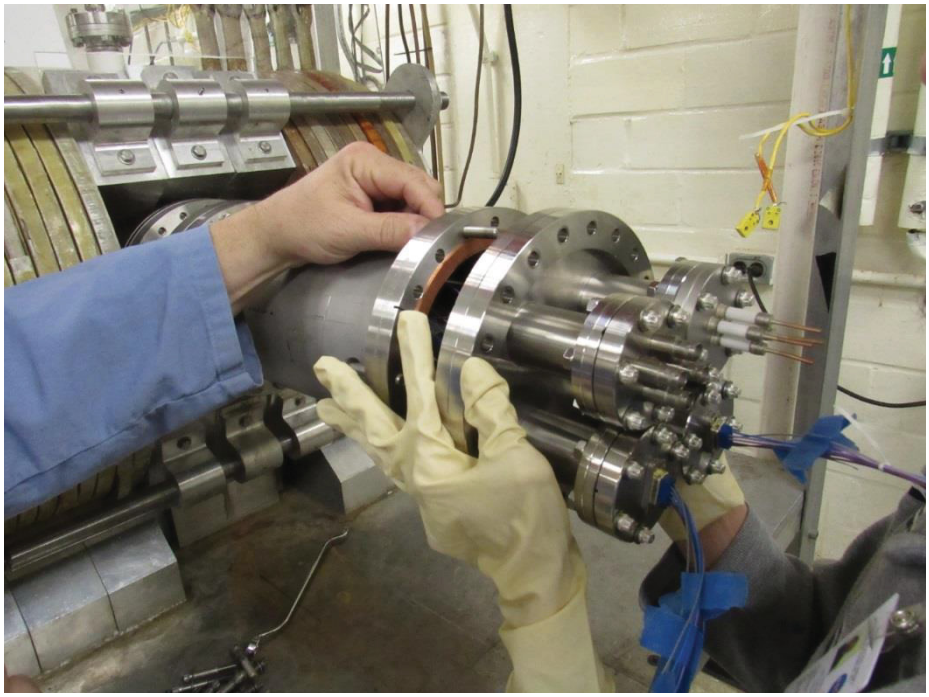

Figure 28: Installation of the REDD mounting system onto the 8 inch CF of the AOF target cavity.

down to $4*10^{-6}$ Torr and the electrical interface is connected to the associated external equipment shown in Figure 29 as detailed in the electrical ICD located in Appendix A. Once the chamber pressure was observed to stabilize, the AOF's power was ramped to 220 V DC to create the magnetic field required to collimate the plasma beam. The appropriate voltage biases were applied as detailed in the electrical ICD in Appendix A, and all Keithley measurement devices

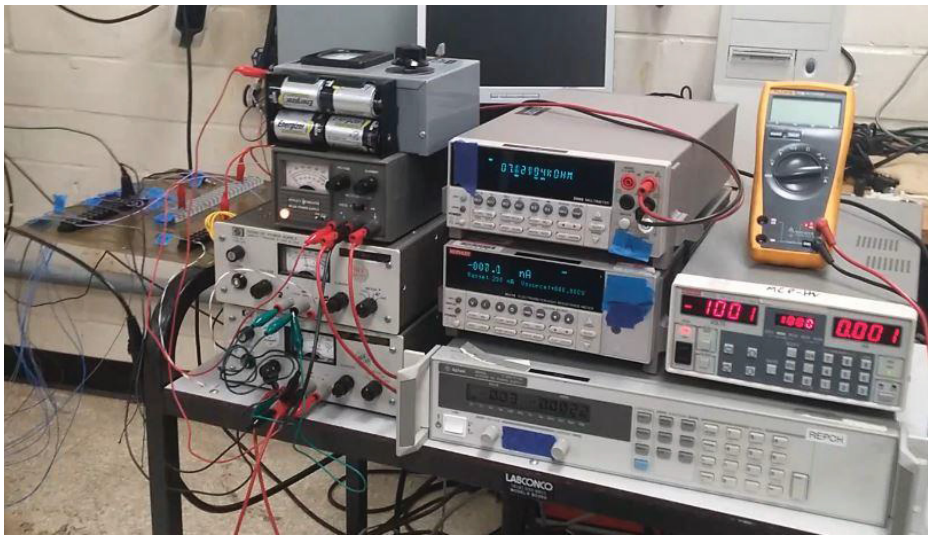

Figure 29: External equipment used in initial end-to-end testing of REDD.

were powered on. The included software NI-Max was then opened to verify the communication of all LabVIEW controlled devices.

The following procedure was followed for end-to-end testing of the device. The REDD GUI was opened and any user-specified parameters pertaining to the upcoming test were entered. At this juncture the AO pulse was engaged and adjusted by the AOF operator to the appropriate duty cycle and energy level. The Keithley 248 high voltage supply was then incrementally ramped up according to the specifications to the needed test value. After this process was completed, all electrical connections outside the chamber were manually checked using a handheld Fluke multimeter to verify that the correct polarities and voltages were observed. Next, the REDD GUI was initialized and the appropriate mode of operation for the upcoming test was selected. The Start button was then pressed to commence data collection. The Reading per Batch value was typically set to 500-1000 to provide long periods of continuous measurement at the maximum sample rate possible. When either the desired retarding voltage sweep was completed, or the desired time to measure current at a single retarding voltage level was reached, the Stop button

was manually pressed. If temperature readings indicated the ionization chamber was exceeding 80 degrees, the Stop button was pressed to avoid damage to the device. The GUI then completed the current batch of measurements, resetting the retarding voltage level to 0 V, and ceased monitoring external equipment. The software then populated the output file with the stored measurements and relevant parameters before ceasing operation. This procedure was repeated for each measurement trial.

When testing reached completion, the GUI was closed, the high voltage supply was incrementally ramped down as detailed in the specifications, and external equipment was powered off. The AO beam was then disengaged and the AOF voltage ramped down slowly over a period of 20 seconds. If further testing was scheduled to occur the next day, all connections remained connected and the chamber was held at vacuum overnight.

Results and Discussion

Magnetic Field Mitigation Testing Results

Magnetic field profile measurements of the AOF at NASA MSFC were made and an optimal location for placement of REDD established during the 2016 summer internship. Further measurements taken during January and May of 2017 showed the magnetic field profile results to be reproducible and repeatable. The mounting system coupled with the passive shielding allows for the fine adjustment of the device location within the area of minimum magnetic interference. The double-layer cylindrical μ-metal shielding was installed with the most magnetically sensitive portion of REDD centered on this null point in the field and probe measurements were repeated along the axis of the beam as seen in Figure 30.

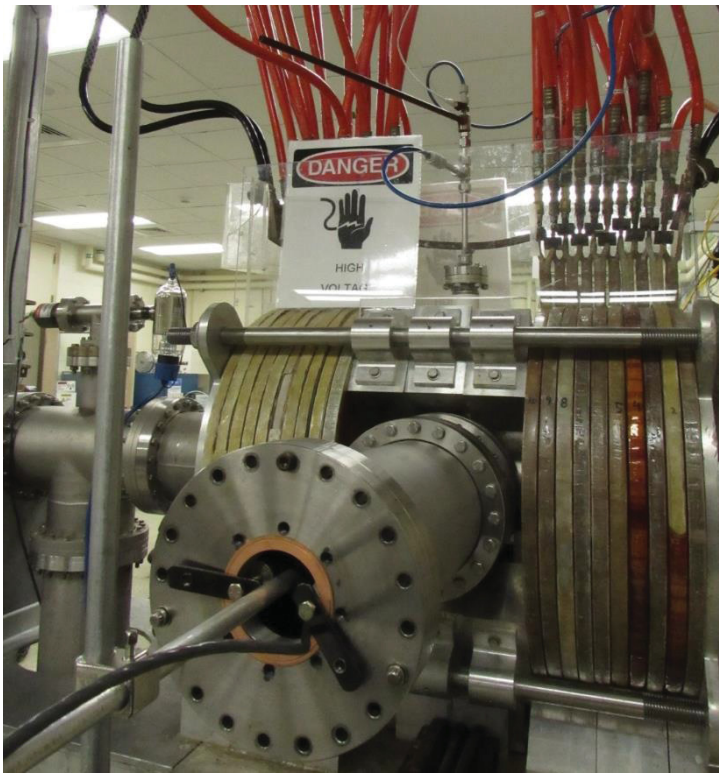

Figure 30: Repeated magnetic field measurements taken after installation of passive shielding system within the AOF. REDD is installed within the shielding system and suppression of the field at the exact location of the device is verified using the Model 460 Kilogauss probe.

Figure 31 presents the comparison of 3-axis field measurements that were made before and after implementation of the shielding, illustrating successful attenuation of the field to Earth ambient levels. It was shown earlier that this area of minimum field magnitude is at the radial distance from the cylinder axis at which the polarity of the Bx and By components changes sign.

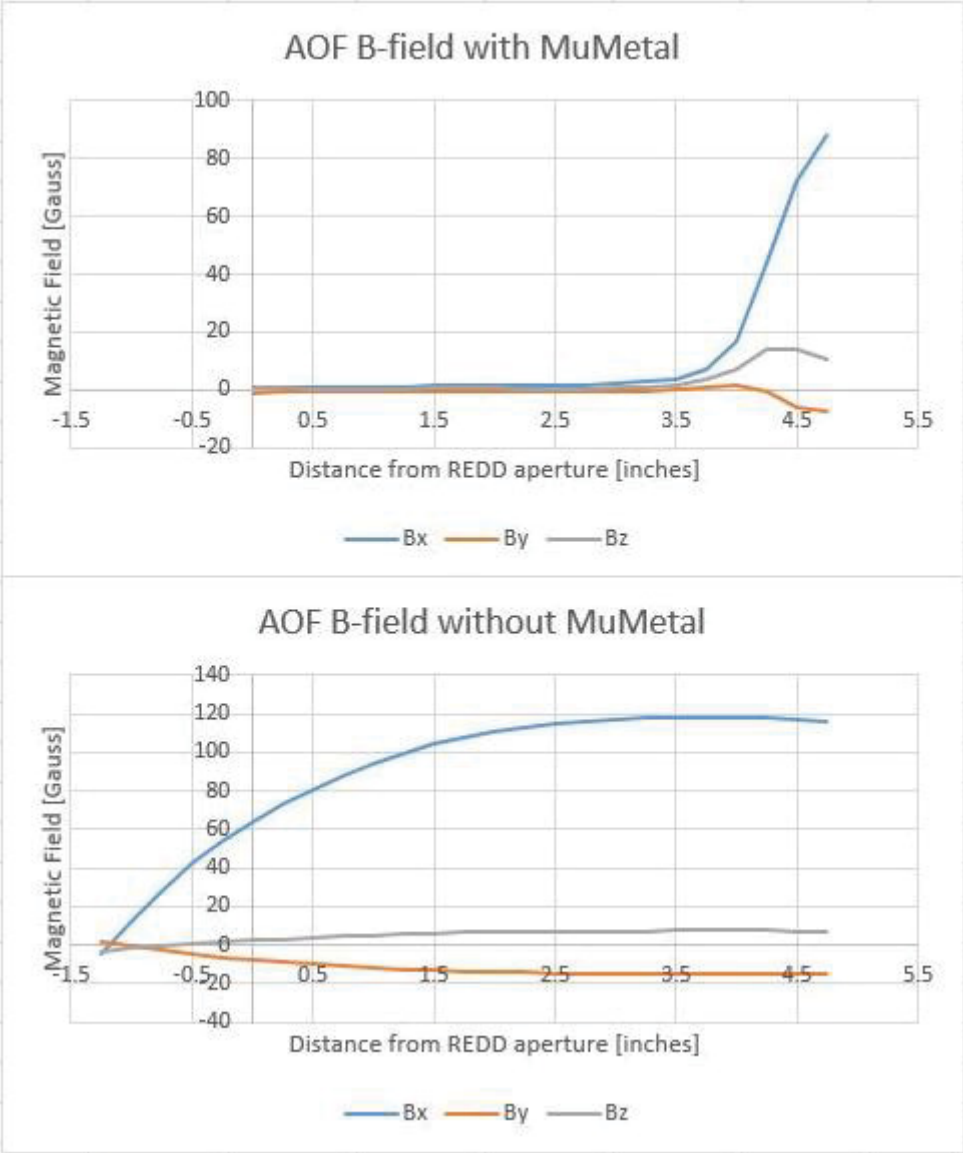

Figure 31: Comparison of all three components of the B-field with respect to the location of REDD within the system. The upper plot shows measurements taken after installation of REDD within the passive shielding system. The lower plot shows B-field measurements taken prior to installing the shielding.

Measurements beginning at this null point and progressing radially outward from the chamber center are shown in the lower plot of Figure 31. The null point can be seen on the far left where all three components converge prior to shielding. The upper portion of Figure 31 shows field measurements in all three components beginning at the REDD aperture, as it was not possible to extend the probe into the sensor itself. As seen in the figure, the passive shielding system significantly reduces both the Bx and By components of the field, so they approach Earth ambient levels. The measurements indicate that the field magnitude is suppressed to ~1 G at the REDD aperture, 3 G at a position 3.5 inches from the REDD aperture, and 1.5 inches past the end of the device. These measurements indicate that the magnetic field components are reduced to levels far below those needed to cause significant effects on the Larmor radius of charged particles within the device.

End-to-End Testing Results

The initial results of end-to-end testing at MSFC shown in Figure 32 show the first large capture of 8,501 samples of the AO pulse by the REDD device. The chamber pressure was lowered to $4*10^{6}$ Torr and the voltage supplying the coils raised to 220 V DC before engaging the pulsed AO beam. MCP output current measurements ranging from -785 nA to -1 nA were recorded during a single run at 120 samples per second. These measurements are within the expected range seen during subsystem testing, and are several orders of magnitude above the 100 pA noise level of the REDD electronics (Venkatramanan, 2015).

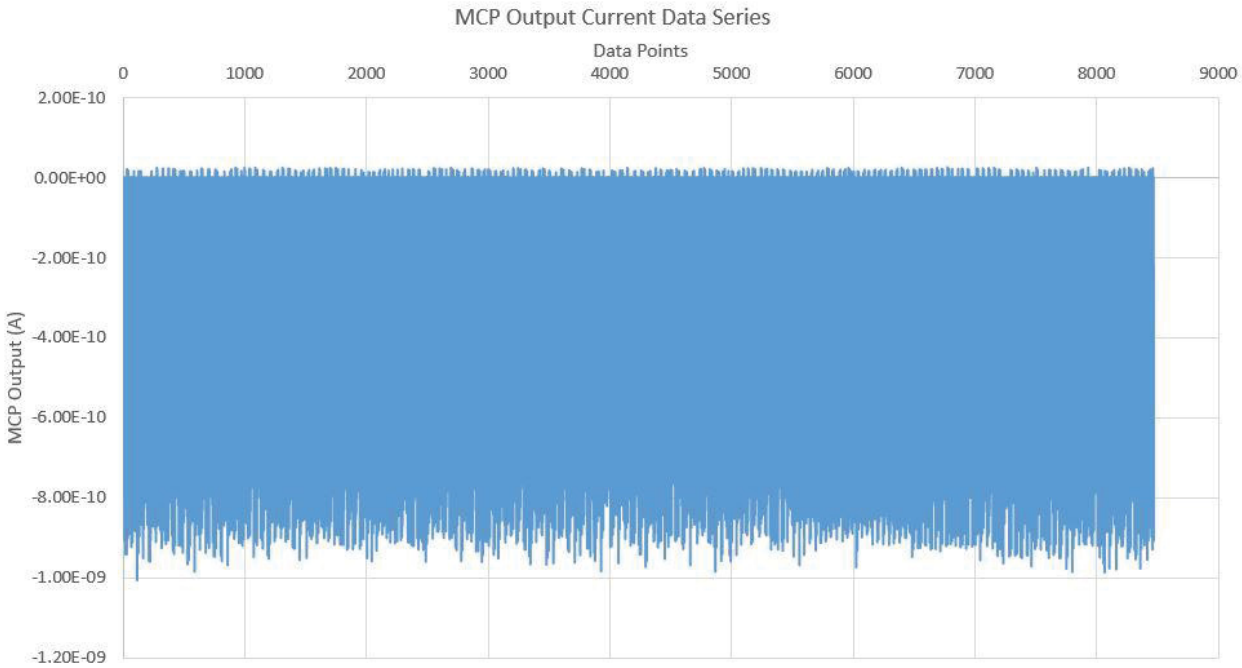

Figure 32: Initial 8,501 sample capture of the AO pulse using large batch measurements.

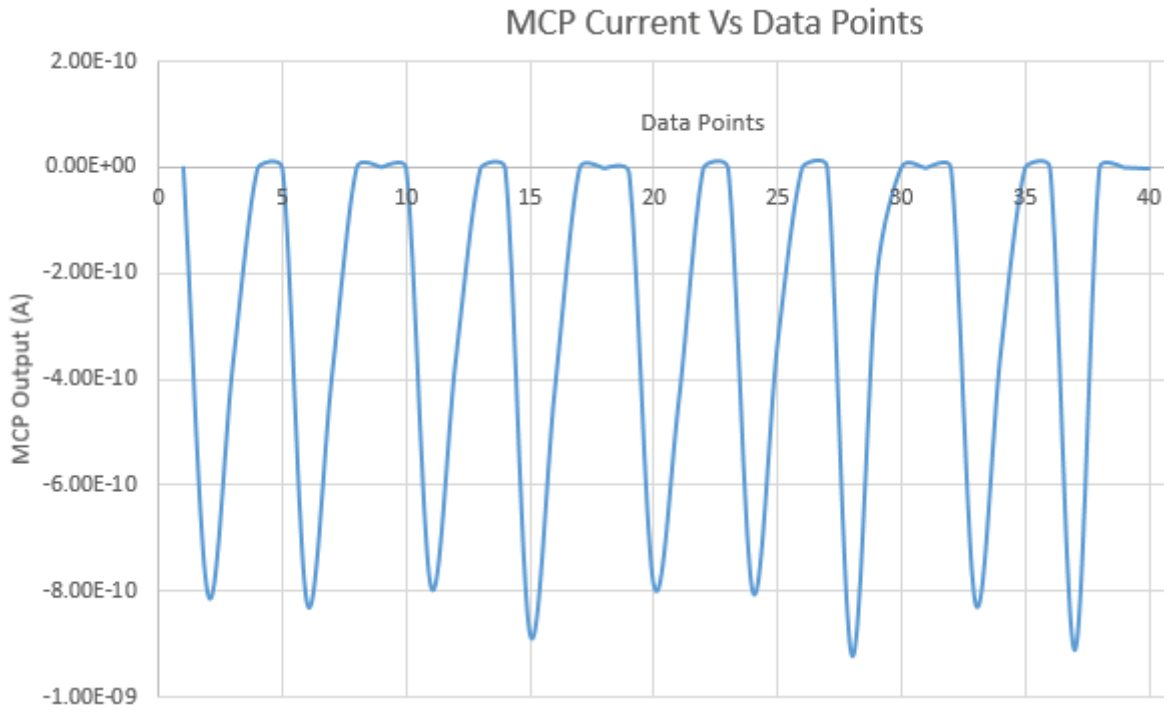

Figure 33: Initial AOF pulse capture. A 39 sample window of MCP output current taken during the initial 8,501 sample capture of the AO pulse is shown above.

A closer view of the initial data series shown in Figure 33 shows a clear view of the AOF pulse over a 40 sample section, confirming the LabVIEW GUI's operation at a sufficient sample rate for capture. This section comprised of data points 76 – 115 of the figure above illustrates the clearly cyclical pattern of the pulse and consistent peak output current level. The end of each pulse exhibits a tapering Gaussian shaped distribution, confirming the expectations of NASA personnel (personal communication, Curtis Bahr).

Additional tests were recorded during several trips to MSFC using varying grid configurations to confirm the functionality of the GUI's sweep mode. The test seen in Figure 34 shows the sweep mode utilized to record the ionization of background gases in the AOF at 125 samples per second. During this test the magnetic field was present and the AO beam disengaged. A direct correlation can be seen between MCP output current in blue and the retarding voltage levels swept from 20 V to 5 V in 2.5 V steps, shown in red. This study of ambient gases in the AOF

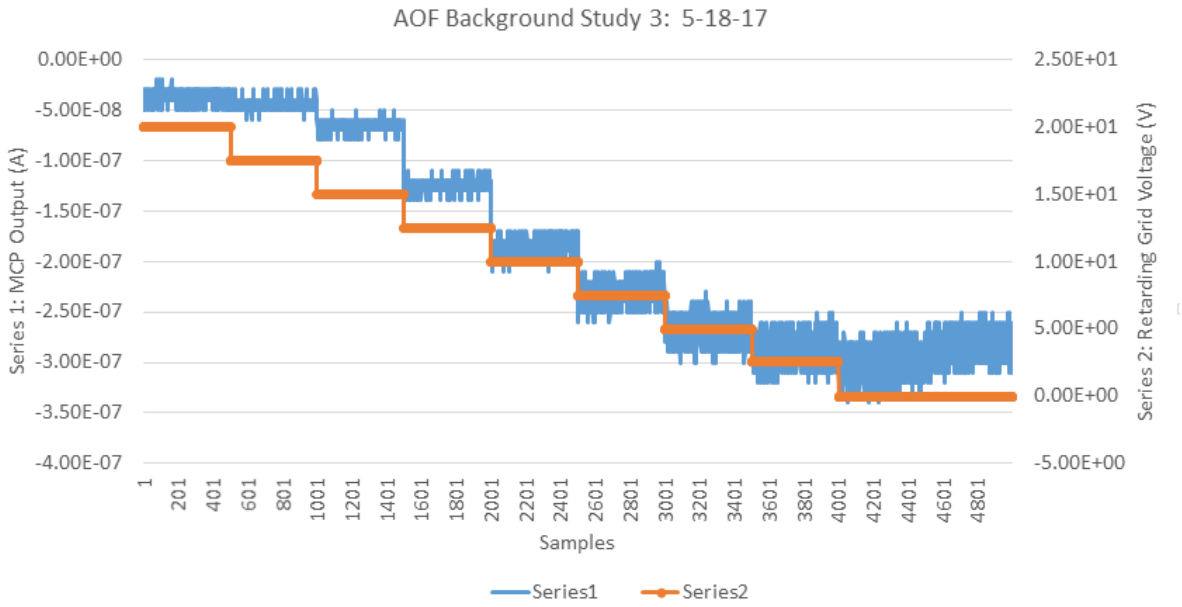

Figure 34: Sweep mode functionality test of background gases present in the AOF with the AO beam disengaged.

vacuum chamber confirms function of the device and provides a background curve that will be used as a control during future validation testing. Repetition of this background test was successful and confirmed operation of the REDD GUI's sweep mode functionality. Figures 35a and 35b show portions of the background test's formatted output file created by the GUI as seen in MS Excel. The portion seen in Figure 35a contains the formatted result of user-specified testing parameters entered in the initial value cluster panel. Figure 35b shows the recorded values for MCP current, retarding grid voltage, and temperature in Celsius; these are outputted to a file along with the formatted date and time of each measurement for subsequent data analysis.

MCP high voltage	MCP low voltage	Extraction Plate 1	Pressure	Ionization Chamber Collector	Filament Circuit Floated Voltage	Extraction Plate 2	Comments for Data Output	Thermistor Starting Temp (C)
							Background noise level test G1: +10 G2: -120 G3: 20:2.5:0 500/batch AO OFF, field OFF	
-2.000000E+3	-70.000000E+0	15.000000E+0	8.000000E-6	0.000000E+0	-110.000000E+0	-15.000000E+0	Fil current at 1.5 A	39.000000E+0

Figure 35a: Example of the formatted file output for the Initial Value Cluster panel populated with user-specified values and comments.

Timestamp	MCP Current (A)	Retarding Grid Voltage (V)	Temperature
10:21:12.00,18-May-2017	-5.00E-08	2.00E+01	3.95E+01
10:21:12.00,18-May-2017	-4.00E-08	2.00E+01	3.95E+01
10:21:12.00,18-May-2017	-4.00E-08	2.00E+01	3.95E+01
10:21:12.00,18-May-2017	-4.00E-08	2.00E+01	3.95E+01
10:21:12.00,18-May-2017	-4.00E-08	2.00E+01	3.95E+01
10:21:12.00,18-May-2017	-3.00E-08	2.00E+01	3.95E+01
10:21:12.00,18-May-2017	-4.00E-08	2.00E+01	3.95E+01
10:21:12.00,18-May-2017	-3.00E-08	2.00E+01	3.95E+01
10:21:12.00,18-May-2017	-3.00E-08	2.00E+01	3.95E+01
10:21:12.00,18-May-2017	-3.00E-08	2.00E+01	3.95E+01
10:21:12.00,18-May-2017	-3.00E-08	2.00E+01	3.95E+01
10:21:12.00,18-May-2017	-4.00E-08	2.00E+01	3.95E+01
10:21:12.00,18-May-2017	-5.00E-08	2.00E+01	3.95E+01
10:21:12.00,18-May-2017	-4.00E-08	2.00E+01	3.95E+01
10:21:12.00,18-May-2017	-4.00E-08	2.00E+01	3.95E+01
10:21:12.00,18-May-2017	-4.00E-08	2.00E+01	3.95E+01

Figure 35b: Example of the formatted file output of the REDD GUI. MCP current, retarding grid voltage, and temperature are recorded in scientific notation. Formatted timestamp is taken from a built-in LabVIEW VI that reads the clock of the computer system being used to operate the GUI.

Conclusion

A LabVIEW-automated testing system to enable testing of the REDD instrument at NASA MSFC has been presented.

The project goals achieved and documented in this thesis include:

1. Design and successful testing of a magnetic shielding system to mitigate the high field strength at the location of the REDD sensor.
2. Fabrication of a custom-made mounting system to hold the REDD sensor and the μ-metal shielding.
3. Development of a LabVIEW GUI to improve the efficiency of the data collection process by allowing quasi-real-time diagnostics during testing.

Figure 36: Photograph of a 5eV pulsed AO beam seen during operation of the MSFC AOF.

The custom-made mount was fabricated and passive shielding implemented to mitigate effects of the strong magnetic field within the system on the trajectories of charged particles within REDD. The LabVIEW GUI developed in this work has been shown to provide sufficient temporal resolution to capture the AO beam seen in Figure 36, and to characterize the instrument responses during pulsed operations. The custom REDD GUI, shown during operation in Figure 37, was successfully developed to provide real-time visual feedback for assessing the effects of various retarding grid voltage levels, bias levels, and system temperature. Visual feedback is given in the form of real-time monitoring for current vs time plots or individual I-V characteristic plots for each retarding voltage sweep. MCP output was monitored through large batch measurements taken by the Keithley 6517b at a resolutions up to 125 samples per second, the maximum rate at which measurements can be internally stored and transmitted through the GPIB. Steinhart-Hart polynomial coefficients are correctly calculated within the script in order to convert temperature-changing resistance values to temperature in degrees Celsius. These measurements were empirically verified using analog monitoring devices. Initial reference values, retarding grid voltages, temperature, and MCP current output were successfully recorded and exported to a spreadsheet format compatible with MS Excel. Sufficient resolution for capture of the pulse was achieved and current levels above the noise level were recorded. These capabilities further end-to-end validation testing at MSFC, which are vital in order to verify REDD's performance specifications and proceed to the next TRL level. A geometry change to provide an increased level of ion distribution within the device has been successfully tested and is scheduled to be implemented in future validation testing.

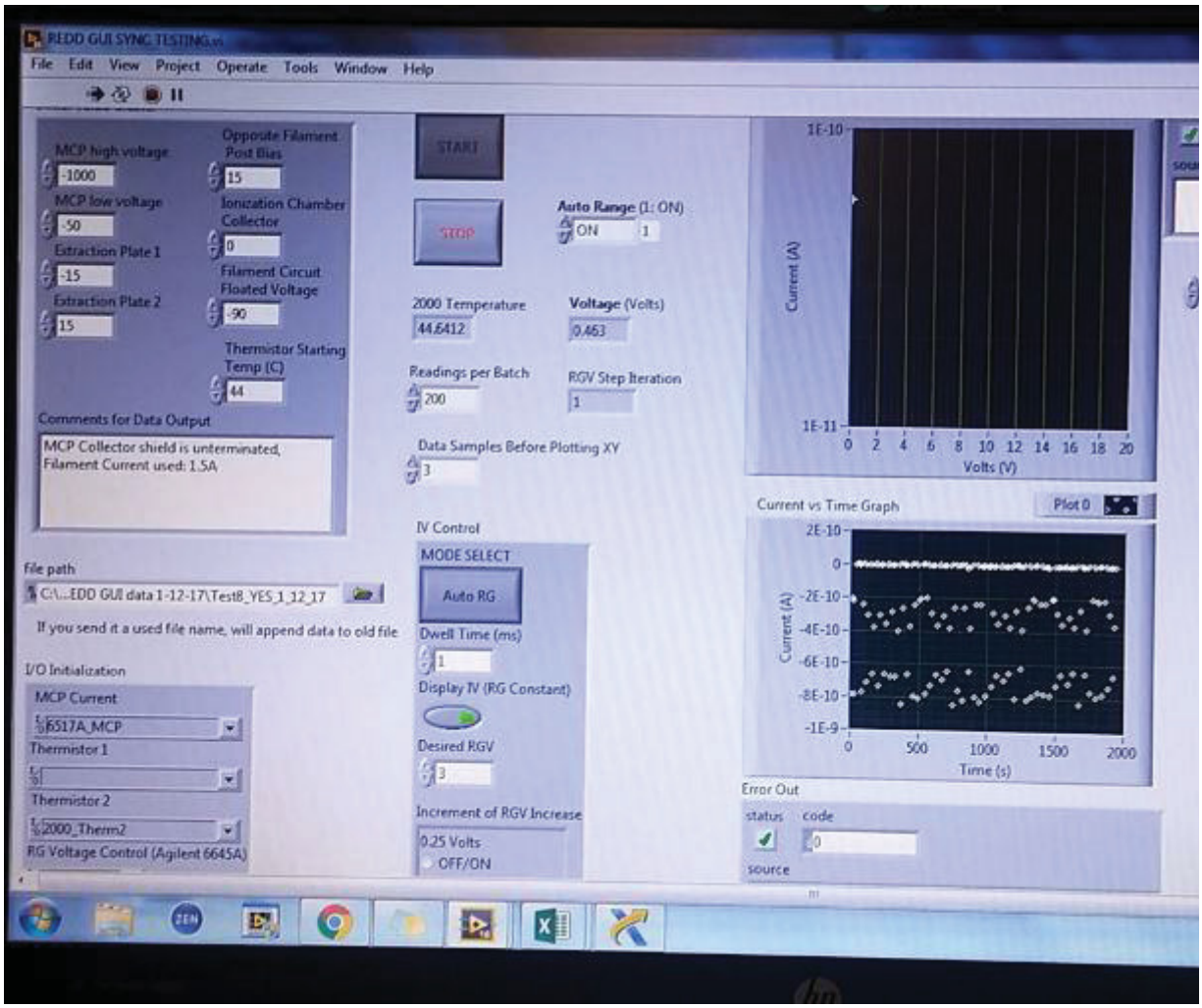

Figure 37: Photograph of REDD GUI during operation

Future Work

Ongoing work by another student will attempt to construct I-V characteristics from data taken using the systems described here. Additional future work will involve the addition of heat sinking to the ionization chamber to enable extended testing periods. Replacing all Kel-F components with a more temperature-resistant material such as ceramic would provide additional resilience to the rapid heating experienced by the device. A method of empirically determining the beam angle of arrival needs to be further tested to ensure proper alignment with the REDD

sensor. Incorporating materials with known degradation rates such as 2 mm Kapton strips to the outer sheath of the device would provide assurance of the AO beam flux rate at the location of the sensor. Syncing Keithley 6517 current measurements with the pulse generator responsible for triggering the AO may be possible using a TTL pulse. Finally, in order to better characterize the AO pulse an increase in the available sample rate is desired. This could be achieved through redesign of the original prototype's electrometer board. Collaboration with AOF personnel and NASA MSFC is ongoing in this effort to validate the sensor, achieve flight ready status, and further promote the use of CubeSats as a viable approach to space science and exploration.

References

1. Cuthbertson, J. W., Langer, W. D., Motley, R. W., & Vaughn, J. A. (1991). Atomic oxygen beam source for erosion simulation.
2. Kordella, L., Earle, G.,(2016). "Creare/Virginia Tech SBIR Project: A CubeSat Compatible Neutral Wind Sensor," unpublished whitepaper, (2016)
3. Fanelli, L., Noel, S., Earle, G. D., Fish, C., Davidson, R. L., Robertson, R. V., ... & Kennedy, P. (2015). A versatile retarding potential analyzer for nano-satellite platforms. *Review of Scientific Instruments*, *86*(12), 124501.
4. Vaughn, J. A., Linton, R. C., Carruth Jr, M. R., Whitaker, A. F., Cuthbertson, J. W., Langer, W. D., & Motley, R. W. (1991). Characterization of a 5-eV neutral atomic oxygen beam facility.
5. Venkatramanan, A., (2015) Design of control electronics for the Ram energy Distribution Detector. Master's thesis, Virginia Tech.
6. Mager, A. (1970). Magnetic shields. *IEEE Transactions on Magnetics*, *6*(1), 67-75.
7. Knudsen, W. C. (1966). Evaluation and demonstration of the use of retarding potential analyzers for measuring several ionospheric quantities. *Journal of Geophysical Research*, *71*(19), 4669-4678.
8. Earle, G. D., Klenzing, J. H., Roddy, P. A., Macaulay, W. A., Perdue, M. D., & Patrick, E. L. (2007). A new satellite-borne neutral wind instrument for thermospheric diagnostics. *Review of Scientific Instruments*, *78*(11), 114501.
9. Bittencourt, J. A. (2013). *Fundamentals of plasma physics*. Springer Science & Business Media.
10. Steinhart, J. S., & Hart, S. R. (1968, August). Calibration curves for thermistors. In *Deep Sea Research and Oceanographic Abstracts* (Vol. 15, No. 4, pp. 497-503). Elsevier.
11. Keithley Instruments, Inc. (2008). Keithley Model 6517B Electrometer Reference Manual (Rev D). Keithley Instruments, Inc.

Appendix A

Electrical ICD

REDD in vacuum						Chamber Interface			
Part Name	Abbr	Function	Wire Color	Gauge	REDD Harnes		Feedthrou gh Inne	Chamber Wall	Outer Harnes
Extraction Plate 1	EX100	+15 bias voltage	red	30 AWG PTFI	1	DB9 1 (PN 110001)	1		1
NC					2		2		2
MCP LV plate	MC101	-100 V max(40-5(	blue	24 AWG PTFI	3		3		3
NC					4		4		4
Extraction Plate 2	EX200	-15 bias voltage	orange	30 AWG PTF	5		5		5
NC(possibly thermistor2)					6		6		6
NC(possibly thermistor2)					7		7		7
Thermistor	TH100	Pos lead	gray	30 AWG PTFI	8		8		8
Thermistor	TH101	Neg lead	brown	30 AWG PTFI	9		9		9
MCP grid high voltage	HV100	-2000 V	W-4210-1806-violet	24 AWG PTFI	1	HV Connector	1		
MCP Collector	MC100	measured current	SMA: remove shielding, run shortest wire possible straight from collector pin		1	MCP Collecting Wire	1		
RV aperture grids	RV100	GND	black	30 AWG PTFI	1	DB9 2 (PN 110001)	1		1
Ion Source (Filament)	IS100	filament bias (-30\	green	28 AWG PTFI	2		2		2
RV grids	RV101	+1 to +20 V bias	white	30 AWG PTFI	3		3		3
NC					4		4		4
RV suppressor/isolator grid	RV102	GND	black	30 AWG PTFI	5		5		5
Ion source Backing Plate	IS102	-100 V max bias	green	28 AWG PTFI	6		6		6
Ionization chamber collector plug	IC101	GND(tied to IC100) or small bias	purple	28 AWG PTFI	7		7		7
Ion Source (Filament)	IS101	filament return	white	28 AWG PTFI	8		8		8
Ionization chamber	IC100	separate GND	black	28 AWG PTFI	9		9		9

Chamber Interface				To External Instrumentation							
Feedthrough Inner		Outer Harness		Breakout Harness	Wire Color	Gauge	Abbr	Function	Device		Control
1	Chamber Wall	1	DB9 connector 1	5	dk. blue	30 AWG PTF	EX100	+15 bias voltage	15-25V DC Power Supply 1 (NASA supplied)		Analog
2		2		4							
3		3		3	gray	24 AWG PTF	MC101	-100 V max bias	100 V DC Power Supply 1 (NASA supplied)		
4		4		2							
5		5		1	lt. blue	30 AWG PTF	EX200	-15 bias voltage	15-25V DC Power Supply 1 (NASA supplied)		
6		6		9							
7		7		8							
8		8		7	dk. purple	30 AWG PTF	TH100	Pos lead	Keithley Electrometer/Ohmmeter (6517A)		LabVIEW GUI (Monitored)
9		9		6	lt. purple	30 AWG PTF	TH101	Neg lead			
1			HV Connector	1	W-4210-1806-violet	24 AWG PTF	HV100		HV Power Supply (Keithley Model 248)		Analog
1			MCP Collecting Wire	1	red?		MC100		Keithley Electrometer 1 - Model 6517B		LabVIEW GUI (Monitored)
1		1	DB9 connector 2	5	gray	30 AWG PTF	RV100	GND	25 V DC Power Supply 2 (Tektronix PS 280)		Analog
2		2		4	lt. blue	28 AWG PTF	IS100	filament bias	Filament Ckt floated with batteries		
3		3		3	lt purple	30 AWG PTF	RV101	+1 to +12 V bias	25 V DC Power Supply 2 (Tektronix PS 280)		LabVIEW GUI (Controlled)
4		4		2							
5		5		1	gray	30 AWG PTF	RV102	GND	25 V DC Power Supply 2 (Tektronix PS 280)		Analog
6		6		9	drk. purple	28 AWG PTF	IS102	-100 V max bias	100 V DC Power Supply 1 (NASA supplied)		
7		7		8	dk. blue	28 AWG PTF	IC101	GND(tied to IC100) or small bias	Ammeter	25 V DC Power Supply 2 (Tektronix PS 280)	
8		8		7	lt. blue	28 AWG PTF	IS101	filament return	Filament Ckt floated with batteries		
9		9		6	gray	28 AWG PTF	IC100	GND	Ammeter	25 V DC Power Supply 2 (Tektronix PS 280)	Analog

Appendix B

LabVIEW Code: Back End

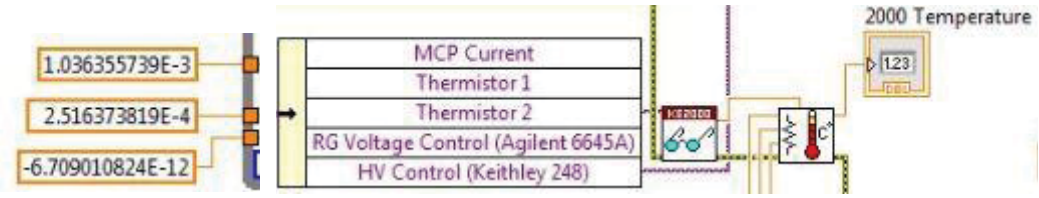

Figure B1: Method for monitoring temperature through the built-in KE2000 VI. The Thermistor Resistance to Temperature VI takes as inputs the recorded thermistor resistance measurements and the coefficients calculated as detailed in the Software section. The VI takes these inputs in double format as opposed to integer. Its output consist of error status, and temperature in degrees Celsius that is simultaneously sent to the real-time display and a shift register that is included in the output file.

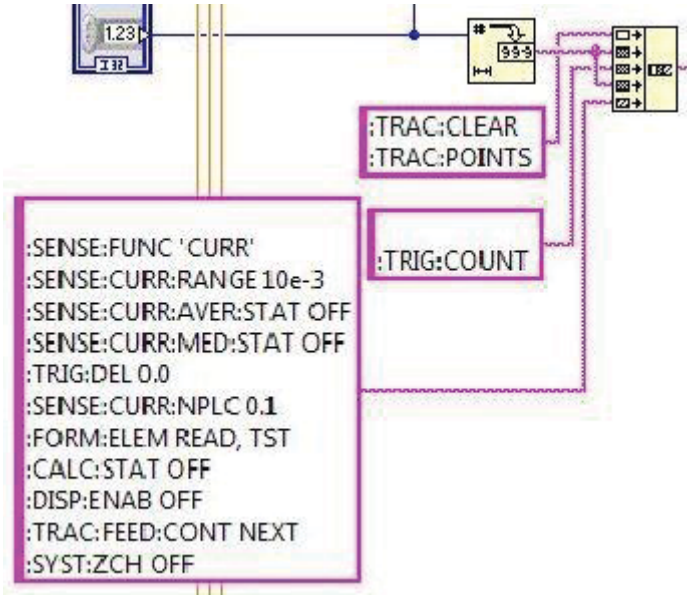

Figure B2: The alteration to Keithley 6517b's standard Trace Buffer VI. To achieve large, controllable speed, batch measurements with only the desired string characteristics the VI takes as input a bundle that includes the user-specified Readings per Batch which is integrated into the native-language commands boxed in purple. These commands control the measurement taken, the range used, filtering, measurement accuracy, calculations, and various setting related to display and speed.

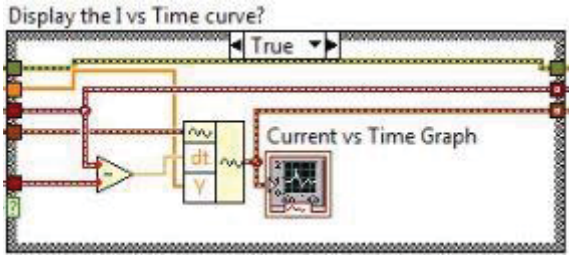

Figure B3: Signal routing to Current vs Time Plot from the IV Control panel. Inputs include current, voltage, timestamp, mean current, and waveform parameters. Current and timestamp outputs continue outside the case structure for data collection as well as errors messages.

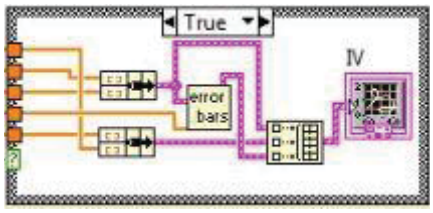

Figure B4: Signal routing for Real-time I-V plotting. Inputs are voltage, current, timestamp, mean current, and standard deviation.